
GEOPOLITICS, GEOFINANCIAL RISK: A MACHINE LEARNING APPROACH*

VERSION OF DECEMBER 1ST, 2025

Alvaro Ortiz
BBVA Research & CRIW(NBER)
alvaro.ortiz@bbva.com

Tomaso Rodrigo
BBVA Research
tomaso.rodrigo@bbva.com

ABSTRACT

We assemble a novel daily panel for 42 advanced and emerging economies over 2018–2025 that combines sovereign CDS spreads, global financial variables, and country-specific news-based indicators of geopolitics, economic and trade policy uncertainty, political tensions, and macro/interest-rate sentiment. Using this dataset, we study how news-based measures shape sovereign risk and how their influence depends on the global financial cycle. First, we run a pseudo–real-time horse race across linear, factor-based, and machine-learning models, comparing a markets-only benchmark (U.S. policy rates and global volatility) with specifications that augment it with news-based indicators, and select the preferred specification strictly on the basis of out-of-sample performance. Across all model classes, adding news improves forecast accuracy, and nonlinear tree ensembles deliver the largest gains; the marginal value of news rises sharply with model flexibility. Second, we interpret the selected model using Shapley and Shapley–Taylor decompositions. Global financial conditions—U.S. policy rates and global volatility—emerge as dominant “push” factors, domestic sentiment explains cross-country dispersion, and geopolitical and geoeconomic variables act as state-dependent amplifiers whose effects peak when global conditions tighten. Third, we map cross-country transmission in the space of Shapley attributions using Diebold–Yilmaz spillovers and network density measures, showing that global financial factors are persistent propagation hubs, whereas geopolitical and policy shocks generate sharp but episodic co-movements. Case studies of the Russia–Ukraine war, the Hamas–Israel conflict, and recent U.S. tariff hikes illustrate these mechanisms in real time and highlight the emerging geoeconomic fragmentation of sovereign risk.

Keywords Geopolitics · GEOFINANCIAL RISK · Machine Learning · Shapley Values · Global Financial Cycle · News Indicators · Non Linearities · Heterogeneity

1 Introduction

Sovereign risk is a central concern for global financial stability, shaping borrowing costs, capital flows, and market resilience to economic and geopolitical shocks. Since the global financial crisis, and especially in recent years, heightened geopolitical and geoeconomic uncertainty has fueled interest in news-based indicators such as Geopolitical Risk (Caldara and Iacoviello, 2022), Economic Policy Uncertainty (Baker et al., 2016), Trade Policy Uncertainty (Caldara et al., 2020), and measures of Political Sentiment (Ahir et al., 2018; Hassan et al., 2019). These indices capture high-frequency shifts in perceptions not fully explained by traditional fundamentals and have been shown to affect investment, asset prices, and sovereign spreads (Novta and Pugacheva, 2021; Boubaker et al., 2023). Our objective is to examine empirically how such sentiment dynamics, together with global financial conditions, are reflected in daily sovereign credit risk, as measured by sovereign credit default swap (CDS) spreads.

To this end, we assemble a novel daily panel dataset for 42 advanced and emerging economies over 2018–2025. The dataset combines local news-based measures of geopolitics (GPR), economic and trade policy uncertainty (EPU, TPU),

*The authors thank, without implicating, Stephen Hansen (UCL), Andreas Joseph (BoE), Juri Marcucci (Banca D’italia), Martin Saldias (Bank of Portugal) and the assistants to the Internal seminar of Bank of Spain and BBVA research. We especially thank to Buket Begun Boga, Patricia Soroa, Pablo Saborido and Ismael Frutos for their contribution to build the database.

and political sentiment with standard drivers such as U.S. monetary policy variables and global volatility proxied by the VIX index. We then conduct a comparative evaluation of linear and nonlinear machine learning (ML) models to identify the specifications that best capture the joint role of market and sentiment factors in sovereign-risk dynamics. Our key objective is to assess the predictive content of news-based indicators and the nonlinear mechanisms through which they interact with global financial conditions.

Existing work has used GPR, EPU, and TPU indices primarily to study macroeconomic aggregates and asset prices, often at monthly frequency and in linear or small-scale VAR frameworks. We add to this literature by bringing country-level, daily, news-based indicators into a unified sovereign risk framework, by running a systematic ML horse race in a high-frequency forecasting setting, and by embedding the resulting models in an interpretability toolkit based on Shapley values, Taylor–Shap interaction indices, and network analysis.

This paper makes three contributions. *First, on the measurement side, we construct a new daily panel that combines sovereign CDS spreads with a harmonized set of news-based indicators of geopolitical risk, economic and trade policy uncertainty, and political sentiment for 42 countries.* This high-frequency dataset allows us to track how global and domestic news are mapped into sovereign credit risk across advanced and emerging economies in real time.

Second, on the forecasting side, we compare linear models, tree-based ensemble methods, and convolutional neural networks in predicting sovereign CDS spreads with and without news-based indicators. We show that incorporating news-based indicators substantially improves out-of-sample forecast performance in our sample, but mainly when nonlinear models are used, suggesting that the predictive value of news operates through interactions and threshold effects that standard linear frameworks—and in particular dimension-reduction approaches such as dynamic factor models—tend to underestimate.

Third, on the mechanisms, we use Shapley value and Shapley–Taylor decompositions, together with network analysis and crisis case studies, to characterize the state-dependent contribution of different drivers to sovereign risk and the heterogeneity of these patterns across countries and regions. We find that global “push” factors such as U.S. rates and global volatility remain central (Calvo et al., 1996; Rey, 2013; Miranda-Agrippino and Rey, 2020), while geopolitical and geoeconomic indicators act as nonlinear amplifiers, especially for emerging Europe and MENA, in line with cross-country differences in trade structures, institutional quality, and external balance-sheet exposures (Maggiori et al., 2020; Didier et al., 2012; Reinhart et al., 2003; Fernández et al., 2018; International Monetary Fund, 2022; Bank for International Settlements, 2022). Narrative analyses of the Russia–Ukraine war, the Hamas–Israel conflict, and the shift in U.S. trade policy after Trump’s election illustrate these mechanisms in concrete episodes.

Throughout, we address interpretability concerns by moving from pure prediction to model-based narratives. After selecting the best-performing specification on out-of-sample criteria, we apply an in-sample decomposition based on Shapley values (Shapley, 1953; Lundberg and Lee, 2017), Shapley–Taylor interaction indices, and network measures to trace state-dependent interactions between global financial conditions and news-based indicators. In doing so, we follow recent calls to use ML methods not as substitutes for structural models but as complementary descriptive tools that uncover complex patterns and interactions in rich, high-frequency data (Mullainathan and Spiess, 2017; Athey, 2018; Varian, 2014).

The paper proceeds as follows. Section 2 details our high-frequency database, combining traditional market variables with a suite of news-based sentiment indices. Section 3 introduces our machine learning framework and its application for model interpretation using Shapley values. Section 4 presents the main empirical findings, evaluating the predictive performance of the models and the insights from the Shapley-based analysis, including the interconnectedness analysis. Section 5 provides a factor decomposition for three major case studies: the Russia–Ukraine war, the Hamas–Israel conflict, and the geoeconomic shock from the shift in U.S. trade policy after Trump’s election. Section 6 concludes.

Related Literature

The determinants of sovereign risk have been studied through diverse lenses, including domestic fundamentals, global financial cycles, and the balance of “push” and “pull” factors. Within this broad field, our analysis highlights the role of news-based indicators—geopolitical, economic, and trade policy uncertainty—as complementary drivers of sovereign spreads. We connect this perspective to work on the Global Financial Cycle and to recent applications of machine learning and network methods to financial markets, with an emphasis on nonlinearities and heterogeneity across countries.

A first body of work has developed news-based measures of uncertainty and sentiment, including economic policy uncertainty, trade policy uncertainty, and geopolitical risk (Baker et al., 2016; Caldara et al., 2020; Caldara and Iacoviello, 2022). These indicators have been shown to influence investment, credit spreads, and asset prices (Hassan et al., 2019; Novta and Pugacheva, 2021), and to help predict conflict and political violence (Mueller and Rauh, 2018,

2022). Recent contributions stress the importance of source selection and text processing, showing that local media can better capture domestic risk perceptions than global outlets (Bondarenko et al., 2024) and that unstructured text carries predictive signals beyond standard fundamentals (Gentzkow et al., 2019; Manela and Moreira, 2017; Davis et al., 2025a; Clayton et al., 2025). We build on this literature by incorporating a broader set of daily news-based indicators—including measures of economic and interest-rate sentiment and political tensions—into sovereign risk models for 42 countries.²

Second, the literature on geopolitics and geoeconomics documents the financial consequences of conflict, sanctions, trade tensions, and global fragmentation. Geopolitical risk has been shown to increase volatility and widen sovereign spreads (Fernández-Villaverde et al., 2024a; Boubaker et al., 2023), while trade tensions and sanctions amplify uncertainty and risk premia with real effects on trade and output (Ahn and Ludema, 2020; Aiyar et al., 2023; Benchimol and Palumbo, 2024; Fernández-Villaverde et al., 2025). Our framework embeds these drivers in a unified empirical analysis of sovereign CDS spreads, allowing us to quantify their contribution relative to traditional market variables.

Third, our paper relates to the literature on “push and pull” factors of capital flows and sudden stops (Calvo et al., 1996, 2004) and to work on the Global Financial Cycle, which highlights U.S. monetary policy and global volatility as key external drivers (Rey, 2013; Fratzscher, 2012; Miranda-Agrippino and Rey, 2020). Recent contributions clarify the transmission channels of these cycles, emphasizing dollar funding conditions, swap lines, and cross-border banking, as well as the fundamental bias of global capital allocation toward dollar assets (Du et al., 2018a; Bahaj and Reis, 2022; Goldberg and Cetorelli, 2020a; Maggiori et al., 2020). We extend this literature by analyzing traditional global “push” factors jointly with domestic conditions and news-based indicators of economic and trade policy uncertainty and geopolitical risk, thereby placing the Global Financial Cycle in a richer informational environment.

Finally, financial markets often display nonlinear dynamics such as thresholds, asymmetries, and regime shifts (Hamilton, 1989; Teräsvirta, 1994; Cont, 2001). Recent work shows that machine learning methods can capture these complexities and improve prediction in crisis forecasting and risk spillovers (Gu et al., 2020; Joseph and Strobel, 2021; Bluwstein et al., 2023), while the literature on financial networks highlights how interconnectedness and topology shape shock transmission (Diebold and Yilmaz, 2014; Battiston et al., 2016). Parallel contributions document heterogeneity across countries and regions, with advanced and emerging markets responding differently to global push factors and with vulnerabilities shaped by institutions, trade structures, and financial integration (Didier et al., 2012; Reinhart et al., 2003; Fernández et al., 2018; International Monetary Fund, 2022; Bank for International Settlements, 2022).

Our contribution relative to these strands is threefold. First, we bring a comprehensive set of daily news-based indicators into a unified sovereign risk framework that jointly accounts for global financial conditions and domestic sentiment across 42 advanced and emerging economies. Second, we use a systematic comparison of linear and nonlinear machine learning models to document how news-based indicators improve out-of-sample forecasts of sovereign CDS spreads, primarily through nonlinear interactions with global push factors. Third, we employ Shapley-based decompositions and network analysis to uncover state-dependent and heterogeneous responses of sovereign risk to geopolitical and geoeconomic shocks, linking the Global Financial Cycle, news-based measures, and country-specific characteristics within a single empirical framework.

2 Data and Measurement

This section provides a description of the high frequency daily database of country risk developed for the empirical analysis used in this work. The database integrates market-based financial indicators with news-based sentiment indicators to explain the performance of the five years sovereign credit default swap (CDS) spreads³, used as a proxy for sovereign credit risk, across 42 countries⁴.

All variables are first smoothed using a 28-day moving average to mitigate daily noise and isolate persistent trends. Subsequently, each series is standardized to have a zero mean and unit variance over its respective sample period for

²These daily indicators are updated weekly at BBVA Research.

³The 5-year sovereign Credit Default Swap (CDS) spread is defined as the annualized premium, expressed in basis points, that a protection buyer pays to insure against a credit event (e.g., default or restructuring) on sovereign debt over a five-year horizon. This maturity is selected as the primary proxy for sovereign credit risk because the 5-year tenor is the most liquid and widely traded segment of the CDS curve, establishing it as the standard industry benchmark for pricing default probability. Furthermore, unlike government bond yield spreads, CDS spreads provide a purer measure of credit risk by isolating default expectations from funding costs, interest rate risk, and bond-specific supply dynamics.

⁴Our sample includes Argentina, Australia, Austria, Belgium, Brazil, Canada, Chile, China, Colombia, Czech Republic (CzechRep), Denmark, Egypt, Finland, France, Germany, Hungary, India, Indonesia, Israel, Italy, Japan, Jordan, Malaysia, Mexico, Morocco, Netherlands, Norway, Peru, Philippines, Poland, Qatar, Russia, Saudi Arabia, Sweden, Spain, Thailand, Turkey, Ukraine, United Kingdom, United States, Uruguay and Vietnam. The countries are classified by region too.

each country. Our analysis uses an unbalanced panel spanning from January 2017 to July 2025; Country-specific data availability, as well as percentile distributions by country, are detailed in Appendix A. This pre-processing ensures comparability across indicators while preserving the informational content of large shocks. Consistent with this objective, we do not perform any outlier treatment, as we consider extreme events to be informative signals of exceptional shifts in risk perception.

Our main contribution in the dataset is the construction of coverage and sentiment-based measures on a daily basis derived from international news sources for some of the explanatory variables. These indicators are produced by BBVA Research using the *Global Database of Events, Language, and Tone (GDELT)*, an open-source platform that monitors and parses global digital media.⁵ Leetaru and Schrodt (2013), GDELT covers broadcast, print, and online outlets in more than 100 languages, updated every fifteen minutes, and provides a high-frequency and wide-coverage record of events worldwide. Articles mentioning relevant topics are identified in their local language, translated into English and processed applying a vast amount of algorithms to create indicators based on total media, foreign media and local sources.

Following Bondarenko et al. (2024), we rely on local media sources rather than foreign media to construct the indicators. Local newspapers provide a more accurate representation of risks and uncertainties are perceived domestically. Bondarenko et al. (2024) captures, for geopolitical risk, heterogeneity in national perspectives, proximity to conflict, and differences in press coverage that global (English-language) media often miss. They show that shocks identified from local news sources have significant effects on domestic financial markets and macroeconomic conditions, whereas shocks based on Anglosphere media tend to underestimate local impacts.

We construct two types of news-based indicators. The first type measures "*Uncertainty*" and is based solely on the volume of relevant news coverage. For our Economic and Trade Policy Uncertainty indices, we follow the methodology in line with the original methodology Baker et al. (2016). Specifically, we compute coverage as the daily share of articles containing a predefined set of uncertainty-related keywords, with the complete keyword lists detailed in the Appendix A. This measure is then normalized by the total volume of daily news for each country to create a robust indicator that accounts for secular trends in media output and processing noise.

The second type of indicator combines *News Volume and Sentiment*. This approach is used to construct our indices for domestic Economic Sentiment (ECO), Local Interest Rate Sentiment (INT), Geopolitical Risk (GPR), and Political Tensions (POL). For these variables, we first compute the average sentiment of all relevant articles. This is achieved by scoring the text with over 40 different GDELT sentiment dictionaries, yielding a tone score typically ranging from -10 (highly negative) to +10 (highly positive). The final index is then the product of this sentiment score and the normalized news coverage. This product is inverted for interpretability, ensuring that a higher index value consistently corresponds to greater risk or more negative sentiment.⁶

The dependent variable is the sovereign credit default swap (CDS) spread. A sovereign credit default swap is a derivative contract in which investors pay a premium to insure against credit events—default, restructuring, or missed payments—on a sovereign’s external, foreign-law bonds. The CDS spread is thus an option-implied measure of sovereign default risk. CDS spreads reflect the cost of insuring against a sovereign default, which are widely used as a market-based measure of sovereign credit risk. CDS spreads provide a comprehensive indicator of how markets assess sovereign risk at a given point in time.

The set of the explanatory variables to explain the sovereign risk fluctuations are included in three groups of variables, representing the global financial conditions, the domestic situation and political and geopolitical framework⁷ :

- Global Financial Variables. To capture global financial conditions, we rely on market data for two key variables, representative of global monetary policy and global volatility:

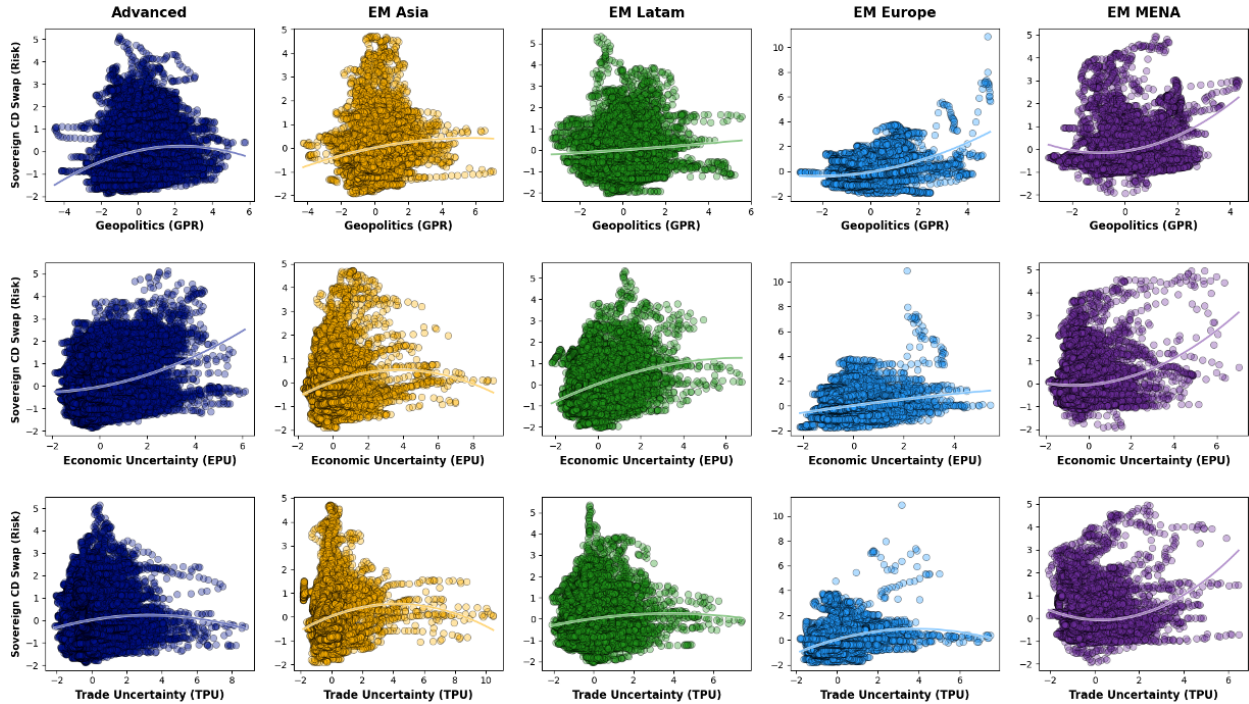
⁵An alternative, and widely used, source for constructing such news-based indicators is the Dow Jones Factiva database. Unlike the open-source GDELT platform, Factiva is a premium, subscription-based archive that provides access to a vast and deeply curated collection of licensed global news sources, news-wires, and trade publications. Its extensive historical data and high-quality sources make it a common choice in academic research for building custom, long-run indicators. For example, the historical component of the widely-cited Economic Policy Uncertainty (EPU) index is constructed using news archives from Factiva.

⁶A detailed description of the keyword sets, dictionaries, and construction formulas for all indicators is provided in the Appendix A. The complete set of daily and weekly indicators is publicly available at our online dashboard: <https://bigdata.bbvareresearch.com/en/>.

⁷Existing work emphasizes structural determinants of external debt dynamics. Our contribution is complementary: we incorporate high-frequency, news-based indicators alongside global financial conditions, domestic macroeconomic settings, and political–geopolitical tensions, all of which bear directly on sovereign default risk.

- *Federal Reserve Policy Rate (FED)*. To avoid the zero policy rate of the federal reserve, we rely on the 2 years yield as suggested by Swanson (2021)) the 2-year US Treasury yield to reflect the cost of government borrowing in the financial market.
- *Global financial volatility (CBOE Volatility Index, VIX)*, which measures implied volatility in the S&P 500 and is commonly referred to as a “fear index,” capturing shifts in global investor risk aversion.
- Macroeconomic sentiment variables. We develop some media-based sentiment indicators about domestic economic activity, monetary policy and economic and trade uncertainty:
 - *The Economic Sentiment Indicator (ECO)* captures the narrative framing of the broader economic environment, as perceived by society, investors, and policymakers, reflecting the narratives and expectations that shape market behavior.
 - *The Interest Rate Sentiment Indicator (INT)*, that reflects perceptions and expectations regarding monetary policy and borrowing costs, quantifying expectations and narratives around monetary policy.
 - *The Local Economic Policy Uncertainty (EPU) Index*, which captures references to ambiguity regarding economic policy decisions in the media.
 - *The Trade Policy Uncertainty Index (TPU)*, which focuses on uncertainty related to international trade rules, negotiations, and disputes.
- *Political and Geopolitical Sentiment variables*. To track political tensions and geopolitical risks, we construct Geopolitical Risk indices as well as Political Risk Sentiment indices, described as following:
 - *The Geopolitical Risk Index (GPR)* reflects the prevalence of international conflict, military disputes, and terrorism.
 - *The Political Tensions Indicator (POL)* emphasizes domestic instability, unrest, and political contestation.

Figure 1: Geopolitics and Geoeconomics News-Based indicators Vs. Sovereign Risk (CD Swaps)



Notes: The figure presents a a gallery of LOESS–smoothed relationships between key Geopolitics and Geoeconomics (economic policy and trade policy uncertainty) indicators and sovereign credit risk (CDS spreads), segmented by global Asset class and EM regions (Advanced, EM Asia, EM Latam, EM Europe, EM MENA). Each row corresponds to one type of uncertainty—Geopolitics (GPR), Economic Policy Uncertainty (EPU), and Trade Policy Uncertainty (TPU)—while columns represent the five regional groups. The scatter points show the raw data after excluding the extreme upper and lower points of data.

Figure 1 plots news-based indicators of Geopolitics and Geoeconomics—*Geopolitical Risk (GPR)*, *Economic Policy Uncertainty (EPU)*, and *Trade Policy Uncertainty (TPU)*—against sovereign CDS spreads for five regions: Advanced

Economies, EM Asia, EM Latin America, EM Europe, and EM MENA. Each panel includes a nonparametric LOESS fit to summarize the average relationship.

The unconditional associations are modest and heterogeneous across regions. For GPR, the fitted curves generally slope upward but remain weak for most regions, becoming more visible only at high levels of geopolitical stress, especially in EM Europe and EM MENA. EPU displays a clearer and more systematic positive association with CDS spreads in emerging markets, while the relationship is comparatively muted for advanced economies. TPU is the noisiest indicator: dispersion is large and systematic patterns are limited to mild upward curvature in a few EM regions.

These scatterplots are therefore best viewed as a descriptive starting point. They suggest that uncertainty indicators are linked to sovereign risk in a weak but upward-sloping and region-specific way, with particularly pronounced patterns in EM Europe and EM MENA and with EPU behaving more systematically than TPU. At the same time, the diffuse clouds of points indicate that unconditional relationships mask important conditioning on global financial conditions and domestic sentiment, so the initial scatters serve as a diagnostic: they reveal where nonlinearities and hidden interactions are likely operating and anticipate the more interpretable relationships that emerge in the SHAP-based decompositions examined in Section 4, where we study marginal and interaction effects after controlling for global volatility, domestic sentiment, and cross-variable nonlinearities.

3 Econometric Framework

This section sets out our empirical strategy for assessing how high-frequency, news-based measures of sentiment and uncertainty shape sovereign risk, as captured by sovereign credit default swaps (CDS). We assemble and preprocess a daily dataset that combines market variables with news-based indicators for 42 countries, and then estimate a *machine-learning horse race* across a broad set of model classes, including linear and regularized regressions, tree-based ensembles, and neural networks. Predictive performance is evaluated in a recursive, pseudo-real time design that uses only information available up to each forecast origin to minimize overfitting (Mullainathan and Spiess, 2017), and we select the preferred specification solely on the basis of its out-of-sample loss. We then hold this model fixed and, to address the “black box” critique, apply Shapley value decompositions (Lundberg and Lee, 2017) to trace how global, domestic, and geopolitical–geoeconomic drivers contribute to sovereign risk over time and to build narratives around major geopolitical and geoeconomic episodes. Finally, we examine cross-country transmission and heterogeneity using two complementary measures of interconnectedness—Diebold–Yilmaz spillovers (Diebold and Yilmaz, 2014) and a nonparametric network-density measure—which allow us to distinguish directional propagation from synchronous co-movement in sovereign risk.

3.1 A Machine Learning Approach

We examine how news-based measures of uncertainty and sentiment shape sovereign risk in a high-frequency setting. Departing from models centered on low-frequency structural fundamentals, our analysis focuses on daily market and news indicators that capture the drivers of country risk: global financial conditions, economic and trade policy uncertainty, macroeconomic and interest-rate sentiment, and geopolitical or political risks. Sovereign risk is proxied by standardized CDS spreads for 42 countries, demeaned and normalized to highlight deviations from country-specific norms and facilitate cross-country comparability. Building on the data framework described above, we hypothesize that sovereign risk reflects the joint influence of global financial variables (such as policy rates and the VIX), domestic macroeconomic conditions, economic and trade policy uncertainty, and political–geopolitical tensions.

To evaluate this hypothesis, we consolidate these drivers into a predictor vector $\mathbf{X}_{i,t}$ for country i at time t and assess their predictive content within a range of machine learning models. Identifying the true form of $f(\cdot)$ is challenging, especially when the relationship between the dependent and explanatory variables may be highly nonlinear (Varian, 2014; Mullainathan and Spiess, 2017). Threshold effects, interactions with fundamentals, and saturation are difficult to capture with standard linear models. To avoid imposing restrictive functional assumptions, we adopt a *machine-learning horse race* that compares a wide range of model classes.

$$y_{i,t+1} = f(\mathbf{X}_{i,t}, \boldsymbol{\lambda}_i) + \varepsilon_{i,t+1}, \quad (1)$$

where $y_{i,t+1}$ is the one-day-ahead standardized CDS spread, $\boldsymbol{\lambda}_i$ are geography dummies capturing country-specific fixed effects, and $f(\cdot)$ belongs to a model class \mathcal{F}_m (linear regression, penalized linear models, tree-based ensembles, or neural networks).

The objective of the horse race is to identify the model class that achieves the best predictive performance in a pseudo-real time setting,⁸ where forecasts are generated recursively using only information available up to period t . Because we work with time-series data in an unbalanced panel, random-sample splits are inappropriate. Instead, we adopt a recursive forecasting framework: at each date the model is re-estimated using past data and used to produce one-step-ahead forecasts, preserving the chronological order and avoiding look-ahead bias. Since variables are measured as 28-day moving averages, observations near train–test cut-offs risk overlap; to prevent leakage, we impose a 28-day buffer around each split so that training and test sets remain strictly separated.

The empirical procedure is as follows. First, models are estimated up to 2021, with hyperparameters chosen by cross-validation inside the training period. Second, forecasts are generated recursively from February 2021 to July 2025, producing one-step-ahead predictions for each country over almost a decade.⁹ Model accuracy is then evaluated by comparing forecasts with realized CDS spreads using mean absolute error (MAE) and root mean squared error (RMSE) on the pooled out-of-sample panel and at the country level. Formal definitions of the loss functions and implementation details are provided in Appendix B.

Crucially, model selection is based *only* on out-of-sample performance. We select the best-performing specification over 2018–2025 using MAE and RMSE computed on the recursive forecasts, and then *freeze* its architecture and hyperparameters. This preferred model is used for all subsequent in-sample Shapley decompositions and network analysis; the explanatory tools are not used to influence model choice, thereby avoiding any “peeking” at the interpretations when selecting the forecasting model.

3.2 Evaluation of Information Content: The Relevance of News-Based Indicators

Embedding news-based indicators into the recursive forecasting framework alongside market benchmarks allows us to evaluate both the incremental value of news and the types of models that extract the greatest predictive gains from their inclusion. The benchmark specification includes only global financial variables: the two-year U.S. Treasury yield as a proxy for global interest rates (FED) and the VIX as a proxy for global financial volatility:

$$\mathbf{X}_{i,t}^{\text{Mkt}} = (\text{FED}_t, \text{VIX}_t).$$

This “Markets-only” benchmark nests and outperforms a simple AR(1) specification in our data, providing a demanding baseline grounded in well-established external drivers of global financial assets and capital flows (Calvo et al., 1996; Rey, 2013; Miranda-Agrippino and Rey, 2020; Fratzscher, 2012).

The augmented specification enriches this baseline with high-frequency, more recently developed news-based indicators: the Geopolitical Risk Index (GPR), Economic Policy Uncertainty (EPU), Trade Policy Uncertainty (TPU), local economic sentiment (ECO), interest-rate sentiment (INT), and political tensions (POL):

$$\mathbf{X}_{i,t}^{\text{Mkt+News}} = (\mathbf{X}_{i,t}^{\text{Mkt}}, \text{GPR}_{i,t}, \text{EPU}_{i,t}, \text{TPU}_{i,t}, \text{ECO}_{i,t}, \text{INT}_{i,t}, \text{POL}_{i,t}).$$

For each model class m , we generate one-step-ahead forecasts under both information sets, obtain forecast errors $e_{i,t+1}^{(m,k)} = y_{i,t+1} - \hat{y}_{i,t+1}^{(m,k)}$ for $k \in \{\text{Mkt}, \text{Mkt+News}\}$, and summarize predictive accuracy using MAE and RMSE. The incremental predictive value of news is captured by the change in these loss measures between the Markets-only and Markets+News specifications; positive reductions in MAE or RMSE imply that news indicators enhance forecast accuracy relative to the FED+VIX baseline. Formal expressions and decomposition of gains across regions and countries are reported in Appendix B. This framework isolates the marginal contribution of news and reveals which forecasting technologies—linear, nonlinear, or deep learning—are most effective in exploiting it.

3.3 Interpretability via Shapley Values

We rely on out-of-sample performance to select the preferred model because this criterion reflects the model’s ability to learn patterns that generalize beyond the estimation sample and guards against overfitting. Once the best-performing specification is identified, we freeze its architecture and hyperparameters and use it in-sample *only* for interpretability. In this second stage, the model is no longer tuned or re-estimated; instead, it serves as a disciplined lens to construct narratives of past episodes in a predictive rather than structural sense.¹⁰

⁸Pseudo-real time means that at each forecast origin we restrict the information set to variables observable up to period t , thereby mimicking the information available to an agent standing at that point in time.

⁹This window ensures that the ability of the models to predict the Russia–Ukraine invasion, the Israel–Hamas conflict, and the tariff shocks following the U.S. election is evaluated out of sample.

¹⁰The Shapley analysis is interpretive rather than causal: it attributes model-implied variation in sovereign risk to input variables, reflecting predictive importance rather than structural identification.

For interpretability, we apply the same specification to contemporaneous sovereign risk,

$$y_{i,t} = f^*(X_{i,t}) + \varepsilon_{i,t},$$

where $y_{i,t}$ is the standardized CDS spread for country i , $X_{i,t}$ stacks global, macro, and political/geoeconomic sentiment inputs (and their lags), and f^* is the best-performing machine-learning model selected in the out-of-sample horse race. To understand the past, we compute Shapley values for every historical observation, obtaining factor- and country-specific attributions $\{\phi_{j,i,t}\}$ that exactly decompose the model-implied component of the spread:

$$\hat{y}_{i,t} \equiv f^*(X_{i,t}) = \phi_0 + \sum_{j=1}^M \phi_{j,i,t},$$

with the residual $\varepsilon_{i,t} = y_{i,t} - \hat{y}_{i,t}$ capturing idiosyncratic variation. This setup lets us trace, *ex post*, how much of each day's realized spread is attributed by the model to each driver and how those attributions evolve across time and countries.

Shapley values provide a rigorous, game-theoretic framework (Shapley, 1953; Lundberg and Lee, 2017) for attributing model predictions to individual input variables.¹¹ They are the only attribution approach that is both *locally accurate* and *consistent*: local accuracy ensures that the sum of feature attributions equals the model's prediction for each observation, while consistency guarantees that if a feature's impact on predictions increases in the model, its attribution cannot decrease. Formally, SHAP represents each prediction $f(x)$ for a given instance x as

$$f(x) = \phi_0 + \sum_{j=1}^M \phi_j(x), \quad (2)$$

where M is the number of features, ϕ_0 is the baseline (average) prediction, and $\phi_j(x)$ represents the marginal contribution of feature j . Because this decomposition can be computed for every observation, we can follow the time-varying relevance of specific drivers (e.g., Geopolitical Risk, VIX, or monetary policy) in shaping sovereign CDS spreads.

Beyond main effects, we use SHAP *interaction values* to quantify pairwise complementarities and threshold behavior. The attribution for feature j can be decomposed as

$$\phi_j(x) = \sum_{i=1}^M \phi_{ij}(x) = \phi_{jj}(x) + \sum_{i \neq j} \phi_{ij}(x), \quad (3)$$

where $\phi_{jj}(x)$ is the main (own) effect and $\phi_{ij}(x)$ captures the joint effect of features i and j (for example, how the influence of Geopolitical Risk depends on the level of VIX). In the next section we use these interactions to document threshold effects and to attribute “spillovers” across variables within the model.

3.4 Measures of Spillovers and Connectedness

To enhance our analysis, we employ two complementary measures of interconnectedness applied to the panel of daily, country-level Shapley values generated by the machine-learning model. The first tool, the *Diebold–Yilmaz Spillover Index (DY)*, captures directional and dynamic propagation of shocks through a parametric VAR-based framework (Diebold and Yilmaz, 2014). The second, a *Network Density Measure* (Newman, 2010), provides a nonparametric view of contemporaneous synchronization across countries, drawing on the financial networks literature (Battiston et al., 2016; Barabási, 2016; Alter and Beyer, 2014). Taken together, the two indices are natural complements: DY highlights dynamic, directional spillovers, while density isolates contemporaneous co-movement without imposing parametric structure.¹²

The DY spillover index quantifies the extent to which forecast error variance in one country's Shapley values is explained by shocks originating in other countries. We estimate a Vector Autoregression (VAR) model for the rolling panel of Shapley values and compute the Generalized Forecast Error Variance Decomposition (GFEVD). The resulting spillover

¹¹Shapley values are computed using the open-source Python package SHAP (<https://shap.readthedocs.io/en/latest/>).

¹²This contrast is crucial for interpretation. Episodes of high density but low DY suggest common shocks that trigger simultaneous responses without clear propagation channels. High DY with modest density points to contagion concentrated in specific bilateral links. Simultaneous increases in both correspond to periods of systemic stress, where shocks both synchronize markets and transmit directionally across borders. We apply both measures in Section 4 to trace how sovereign risk interconnectedness evolved during major geopolitical and financial episodes.

matrix $\Theta(H)$ summarizes how much each country contributes to the variance of others at horizon H . The DY index is then defined as the normalized sum of the off-diagonal elements of $\Theta(H)$:

$$S(H) = \frac{1}{N} \sum_{\substack{i,j=1 \\ i \neq j}}^N \tilde{\theta}_{ij}(H) \times 100, \quad (4)$$

where $\tilde{\theta}_{ij}(H)$ denotes the normalized contribution of country j to the forecast error variance of country i . High values of $S(H)$ indicate stronger cross-country transmission of shocks in the Shapley attribution space.

As a robust and complementary perspective, we compute a *Weighted Network Density* statistic that captures the intensity of contemporaneous co-movement, independent of parametric dynamics. Specifically, we calculate pairwise Spearman rank correlations of Shapley values across countries and retain links whose absolute correlation exceeds a threshold τ . Formally, the weighted density is defined as:

$$D_w(\tau) = \frac{\sum_{i=1}^{N-1} \sum_{j=i+1}^N |\rho_{ij}| \cdot \mathbf{1}_{|\rho_{ij}| \geq \tau}}{\frac{N(N-1)}{2}}, \quad (5)$$

where $|\rho_{ij}|$ is the absolute correlation between countries i and j , and $\mathbf{1}_{|\rho_{ij}| \geq \tau}$ indicates whether the link exceeds the threshold. This measure is model-light and nonparametric: it requires no assumptions about lags or forecast horizons and remains robust even in short rolling samples where VAR estimates can be unstable.

Taken together, these indices capture distinct aspects of interconnectedness. DY measures directional spillovers, while density reflects synchronous co-movement. Episodes of high density but low DY suggest common shocks or global news bursts without clear propagation channels; high DY with modest density points to contagion concentrated in specific links; simultaneous increases in both correspond to periods of systemic stress. This dual-metric framework thus provides a richer and more policy-relevant picture of cross-country risk linkages.

4 Empirical Results

4.1 Performance of Machine Learning Models

The empirical evaluation compares alternative model classes using a pseudo-real-time forecasting design with a recursive train–test split to avoid look-ahead bias and leakage around moving-average windows. Table 1 reports out-of-sample forecast accuracy, assessed through mean absolute error (MAE) and root mean squared error (RMSE). Given the strong nonlinearities and heterogeneous dynamics of sovereign spreads, MAE values are relatively high in absolute terms, but the ranking across models is stable and robust.

Four performance tiers emerge across model classes:

- *Ensemble tree methods dominate.* Extremely Randomized Trees achieve the lowest forecast errors, followed by Random Forests, Bagging, Multilayer Random Forests, and Gradient Boosting. These nonlinear ensembles outperform other approaches because they flexibly capture interactions, threshold effects, and state dependence in sovereign-risk dynamics.
- *Convolutional Neural Networks (CNNs) deliver intermediate accuracy.* Deep CNNs clearly outperform linear benchmarks, especially in terms of MAE, while shallow CNNs perform comparably to the better regularized linear and factor-augmented specifications. However, their gains remain smaller than those of tree ensembles, consistent with the limited advantage of convolutional architectures when predictors are relatively smooth macro-financial aggregates rather than raw high-frequency images. .
- *Linear reduction methods provide modest improvements.* Factor-Augmented Regressions and Principal Component Regression typically outperform pure linear models but remain below CNNs and well below ensemble methods (Stock and Watson, 2002; Jolliffe, 2002). Dimension reduction helps mitigate noise but cannot accommodate nonlinear interactions or regime dependence.
- *Linear benchmarks underperform.* OLS, Ridge, Lasso, Elastic Net, and Quantile Regression yield the highest forecast errors. Quantile Regression, estimated at the conditional median, is somewhat more robust to outliers and fat-tailed residuals than OLS, but its performance remains well below that of tree-based methods. Regularization and robustness reduce variance and sensitivity to extremes, yet they cannot offset the specification bias arising from linear functional forms in the presence of nonlinear data-generating processes (Hastie et al., 2009; Koenker and Bassett, 1978).

The ranking is consistent with evidence that economic prediction problems feature strong nonlinearities, high-order interactions, and structural breaks (Varian, 2014; Mullainathan and Spiess, 2017; Gu et al., 2020). Tree-based methods perform well because they partition the predictor space flexibly and handle heterogeneous data types (Breiman, 2001; Goulet Coulombe et al., 2022). Similar findings arise in early-warning and systemic-risk applications (Bluwstein et al., 2023). CNNs offer intermediate gains, while linear benchmarks perform least well. Quantile Regression provides an additional robustness check, targeting the conditional median rather than the mean, but its forecast accuracy remains closer to other linear specifications than to the best-performing ensemble methods, underscoring that robustness to outliers is not a substitute for modeling nonlinearities.

Predictive value of news-based variables.

In forecasting sovereign CDS spreads, a simple autoregressive benchmark is dominated by a more economically meaningful alternative: a *Markets-Only* model using the two global drivers most consistently shown to explain short-run movements in sovereign risk—the U.S. 2-year yield and global financial volatility (VIX). This benchmark nests the persistence captured by an AR(1) while incorporating the external “push factors” highlighted in the global-financial-cycle literature.¹³

Table 1 compares the Markets-Only benchmark with an extended *Markets+News* specification that augments financial variables with text-based measures of geopolitical risk, economic policy uncertainty, trade policy uncertainty, and macroeconomic sentiment.

Table 1: Machine Learning Models Forecast Accuracy: Markets-Only vs. Markets+News (2018–2025)

Machine Learning Model	Benchmark Market Only		News Extended Market + News		Difference (News Extended vs Benchmark)			
	RMSE	MAE	RMSE	MAE	Diff	% Var	Diff	% Var
Linear Regression	1.09	0.92	1.03	0.86	-0.06	-5.7%	-0.06	-6.4%
Lasso	1.03	0.87	0.95	0.80	-0.08	-8.0%	-0.08	-8.7%
Ridge	1.09	0.92	1.02	0.85	-0.07	-6.4%	-0.07	-7.2%
Elastic Net	1.04	0.88	0.95	0.79	-0.09	-8.8%	-0.08	-9.5%
Quantile Linear Regression	0.93	0.77	0.90	0.74	-0.03	-3.7%	-0.03	-4.5%
Principal Components (PCR)	1.09	0.92	0.99	0.82	-0.09	-8.6%	-0.09	-10.3%
Factor Models (FAR)	0.92	0.75	0.88	0.72	-0.04	-4.4%	-0.03	-3.6%
Gradient Boosting	1.00	0.81	0.85	0.67	-0.14	-14.2%	-0.14	-17.9%
Bagging	1.03	0.83	0.84	0.67	-0.19	-18.3%	-0.17	-20.1%
Random Forest	0.99	0.75	0.82	0.65	-0.17	-17.1%	-0.11	-14.3%
Extremely Randomized Trees	0.98	0.74	0.80	0.60	-0.18	-18.5%	-0.14	-19.0%
Multilayer Random Forest (1S)	0.97	0.75	0.84	0.62	-0.13	-13.6%	-0.13	-17.2%
Multilayer Random Forest (2S)	1.01	0.77	0.85	0.65	-0.16	-15.9%	-0.12	-15.5%
Shallow CNN	1.05	0.84	0.97	0.77	-0.09	-8.3%	-0.07	-8.8%
Deep CNN	1.04	0.77	0.89	0.66	-0.15	-14.1%	-0.11	-14.3%

Notes: The table reports out-of-sample root mean squared error (RMSE) and mean absolute error (MAE) for one-day-ahead forecasts of sovereign CDS spreads under two information sets: a Markets-Only benchmark (2-year U.S. Treasury yield and VIX) and an extended specification that augments market variables with news-based indicators (GPR, EPU, TPU, ECO, INT, and POL). All models are estimated in a pseudo-real-time recursive framework with a 28-day buffer to avoid look-ahead bias. “Diff” denotes the change in RMSE or MAE relative to the Markets-Only benchmark (negative values indicate improvements). Percentage differences are computed relative to the Markets-Only model.

Three main findings emerge:

- *Systematic gains across models.* All fourteen models improve when news variables are included. Even linear specifications achieve RMSE reductions of **5–9 percent**, indicating that news-based indicators contain information not embedded in contemporaneous market variables.
- *Larger improvements in nonlinear methods.* The strongest gains occur in tree ensembles. Extremely Randomized Trees reduce RMSE by nearly **19 percent**, while Bagging and Random Forests deliver improvements

¹³ AR(1) forecasts perform worse than the Markets-Only benchmark, confirming that the latter provides a stricter and more informative reference point for evaluating the incremental value of news.

in the 15–18 percent range. These gains confirm that the predictive content of news operates partly through nonlinear interactions that flexible methods are able to exploit.

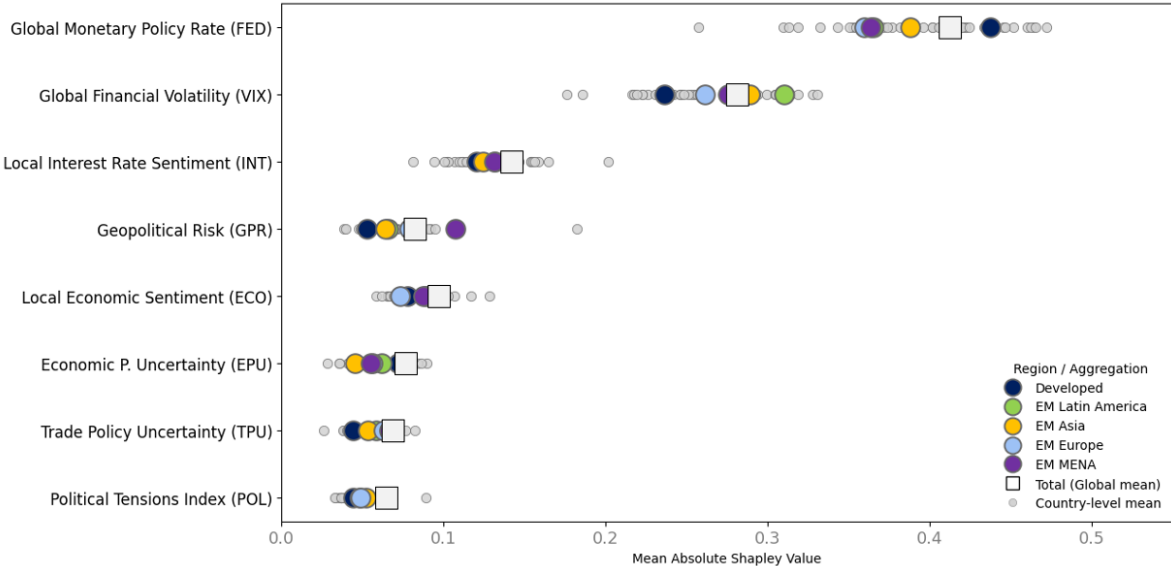
- *Tree ensembles dominate.* Across specifications, ensemble methods deliver the largest accuracy gains and the lowest overall error levels, highlighting their capacity to extract value from noisy, high-dimensional textual indicators.

These results imply that news-based variables capture dimensions of sovereign risk not fully priced by market-based predictors (Baker et al., 2016; Caldara and Iacoviello, 2022). The strength of the improvements is nonlinear: gains scale with a model’s ability to accommodate interactions, state dependence, and threshold effects. This parallels recent evidence that unstructured textual information contains economically meaningful predictive signals beyond standard fundamentals (Gentzkow et al., 2019; Manela and Moreira, 2017; Davis et al., 2025a). More broadly, the findings underscore that the predictive value of news depends critically on both the selection of indicators and the flexibility of the underlying model. Linear methods deliver modest but positive gains, whereas nonlinear approaches extract substantially richer information, consistent with modern perspectives on economic forecasting (Varian, 2014; Mullainathan and Spiess, 2017; Athey and Imbens, 2019).

4.2 Drivers of Sovereign Risk (Shapley Values)

Figure 2 summarizes the model’s feature importance using global, regional, and country-level Shapley values, revealing a clear hierarchy in the drivers of sovereign risk. The figure merges all three levels of aggregation into a single panel, where each marker reports the mean absolute Shapley value of a given predictor over 2018–2025. Squares represent the global average, colored dots the regional means for Advanced Economies, EM Latin America, EM Asia, EM Europe, and EM MENA, and gray circles the corresponding country-level means. This representation allows a unified assessment of how much each variable contributes, on average, to explaining cross-sectional and time variation in sovereign CDS spreads. Three findings stand out.

Figure 2: Variable Importance in Risk Models: Global, Regional, and Country-Level (Shapley Values, 2018–2025)



Notes: The figure reports mean absolute Shapley values for all predictors over 2018–2025, consolidating global, regional (Advanced Economies, EM Latin America, EM Asia, EM Europe, EM MENA), and country-level averages into a single panel. Each marker represents the average absolute contribution of a predictor to sovereign CDS spreads. Colors denote regional groups, squares indicate the global mean, and gray circles represent individual-country means. The horizontal axis shows the magnitude of mean absolute Shapley values; the vertical axis lists all explanatory variables included in the model.

- *Global financial “push” variables dominate.* The global monetary policy rate (proxied by the two-year U.S. Treasury yield) and global financial volatility (VIX) are by far the most influential predictors across all levels of aggregation. Their mean absolute Shapley values exceed those of any other variables for nearly all countries and regions, confirming that the global financial cycle sets the baseline level of sovereign risk. This pattern is

consistent with the literature emphasizing the central role of U.S. monetary policy and global risk appetite in shaping capital flows and risk premia (Rey, 2013; Miranda-Agrippino and Rey, 2020). The large contribution of the VIX corroborates its role as a barometer of global risk aversion, with spikes in volatility historically preceding capital-flow reversals and widening sovereign spreads (Gelos et al., 2011). Recent evidence on dollar funding and international banking—such as Du et al. (2018a), Bahaj and Reis (2022), and Goldberg and Cetorelli (2020a)—provides a micro-founded rationale for this dominance, documenting how U.S. policy and volatility shocks propagate through global funding and banking channels.

- *Domestic macro-financial “pull” variables play a central but more heterogeneous role.* Local interest-rate sentiment (INT) and local economic sentiment (ECO) consistently rank just below the global variables in terms of mean Shapley values. Their contributions are sizeable for both advanced and emerging markets, but display greater dispersion across regions and countries than those of FED and VIX. This indicates that, conditional on the global financial cycle, country-specific macro-financial sentiment is critical for cross-sectional differentiation in spreads (see, for example, Eichengreen et al., 2021a). Countries perceived as having credible, countercyclical monetary and macroeconomic policies exhibit lower Shapley contributions from INT and ECO, and thus lower average CDS premia, even under similar global conditions.
- *Geopolitical and policy-uncertainty indicators are clearly priced but secondary in magnitude on average.* The Geopolitical Risk Index (GPR) exhibits nontrivial contributions, especially in conflict-exposed regions. Economic Policy Uncertainty (EPU) and Trade Policy Uncertainty (TPU) also add explanatory power, in line with evidence that uncertainty about economic or trade policy deters investment and raises credit risk premia (Baker et al., 2016; Caldara et al., 2020). The Political Tensions Index (POL) displays the lowest mean Shapley values, but remains relevant in countries where political instability is salient. Importantly, the dispersion of GPR, EPU, and TPU across EM Europe and MENA is much larger than in Advanced Economies or EM Asia and Latin America, foreshadowing the state-dependent and region-specific nonlinearities documented below. Thus, while their average contribution is smaller than that of global and domestic macro-financial variables, geopolitical shocks can generate large and, for directly affected countries, potentially persistent shifts in sovereign risk.

Overall, the Shapley evidence points to a layered structure: *global financial conditions anchor the level of sovereign risk, domestic macro-financial sentiment differentiates countries within that global environment, and geopolitical or policy-related indicators act primarily as secondary amplifiers.*

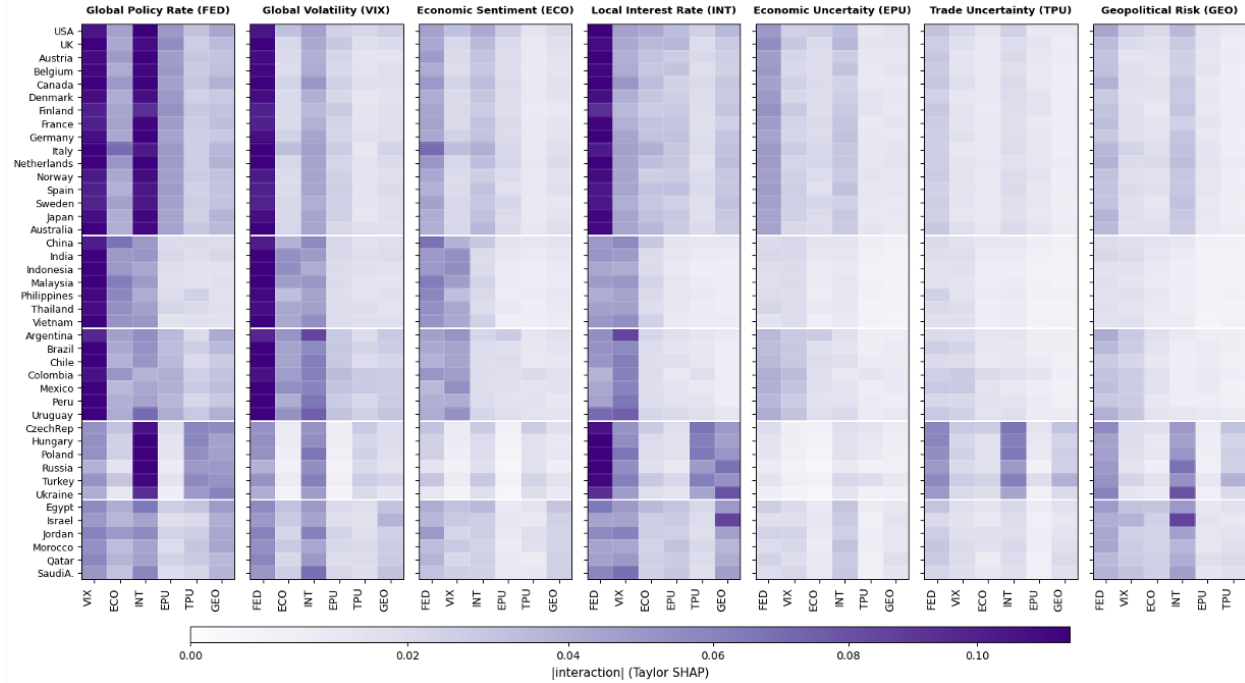
To move beyond average effects, we exploit *Shapley–Taylor interaction values* to measure how the contribution of each predictor depends on the state of the others. Figure 3 reports the resulting interaction intensities at the country level. For each focal variable (panel), the heatmap shows, for all 42 countries, the magnitude of the second-order Taylor–SHAP term with every other predictor; darker shading indicates stronger nonlinear interactions. Countries are ordered by region (Advanced Economies, EM Asia, EM Latin America, EM Europe, EM MENA), allowing a direct comparison of interaction structures across the global sovereign-risk map.

The interaction analysis delivers three further results:

- *Global financial conditions are the dominant source of nonlinear amplification.* Interactions involving the global policy rate (FED) and global volatility (VIX) are systematically the largest across countries. FED×VIX and FED×INT terms are particularly pronounced, indicating that the marginal effect of a policy-rate shock on CDS spreads is much stronger when volatility is high or when domestic interest-rate sentiment is unfavorable. Symmetrically, the impact of volatility shocks is amplified under tight global policy and weak domestic conditions. Thus, the global financial cycle not only has the largest first-order effect; it also governs the strength of higher-order complementarities.
- *Uncertainty and geopolitical variables operate primarily through interactions rather than direct channels,* and these interactions are highly uneven across regions. For most Advanced Economies and for many EM Asia and Latin America countries, the EPU, TPU, and GPR panels display relatively weak interactions, consistent with their modest mean Shapley values. By contrast, interaction intensities are markedly higher in Emerging Europe and MENA. For countries such as Hungary, Poland, Russia, Turkey, Egypt, Israel, and several Gulf economies, EPU and TPU interact strongly with global financial variables (FED, VIX) and with domestic sentiment (INT, ECO), while GPR exhibits pronounced interactions with both global and domestic drivers. This pattern implies that uncertainty and geopolitical news are *state-dependent risk factors*: they become strongly priced when they coincide with tight global financial conditions or weak domestic fundamentals, but their marginal impact is limited in benign environments.
- *Emerging markets display more diffuse and interconnected interaction structures than Advanced Economies.* Advanced Economies’ interactions are concentrated around global financial variables and domestic macro-

Figure 3: Country-Level Taylor–SHAP Interaction Effects of Global, Domestic, and Geopolitical Drivers, 2018–2025

Taylor–SHAP interaction values, 2018–2025



Notes: The figure displays heatmaps of Taylor–SHAP interaction intensities between each core driver and all other variables at the country level. Each panel corresponds to one “key” variable—Global Policy Rate (FED), Global Volatility (VIX), Economic Sentiment (ECO), Local Interest Rate (INT), Economic Uncertainty (EPU), Trade Uncertainty (TPU), and Geopolitical Risk (GPR). Within each panel, rows represent countries, ordered by region (Advanced Economies, Emerging Asia, Latin America, Emerging Europe, and MENA), and columns represent the remaining variables in short-label form. The color scale measures the absolute value of the interaction term, with darker shades indicating larger $| \text{interaction} |$ (Taylor–SHAP) values.

financial sentiment, with relatively limited roles for GPR, EPU, and TPU. In contrast, emerging-market regions—especially EM Europe and EM MENA—exhibit richer networks of interactions spanning global, domestic, and geopolitical/geoeconomic indicators. Sovereign spreads in these countries depend not only on exposure to global shocks but also on the alignment between global conditions and local fundamentals. Misalignments—tight global funding combined with weak domestic sentiment or heightened geopolitical risk—generate disproportionately large nonlinear responses, consistent with evidence on the state-dependent vulnerability of emerging markets to global risk and capital-flow reversals (e.g. Hale et al., 2020a; Broner and Varela, 2017).

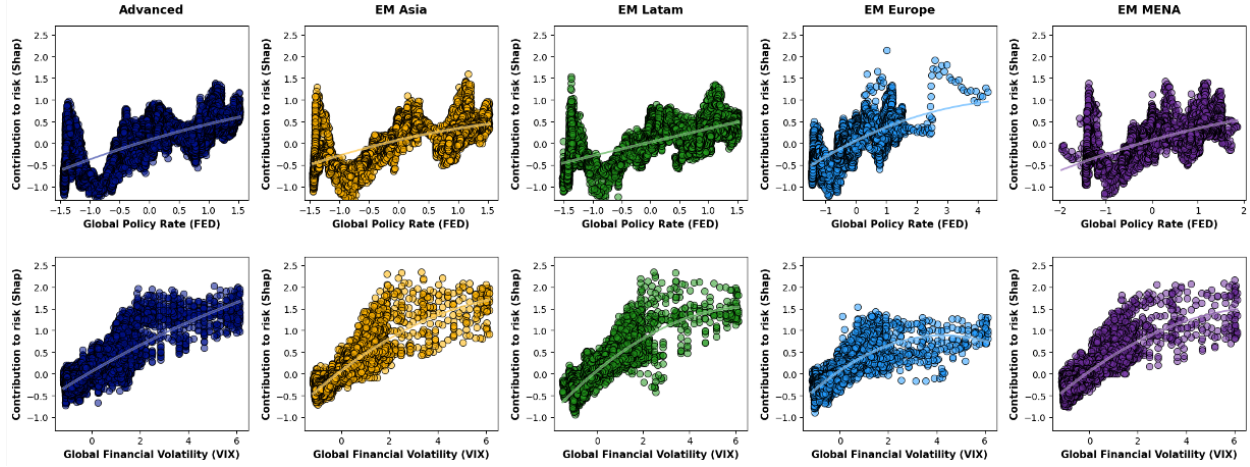
Taken together, the Shapley and Taylor–SHAP results show that sovereign risk is shaped by *nonlinear complementarities rather than purely additive effects*. Global financial conditions provide the main anchor, but domestic macro-financial sentiment and geopolitical or policy-uncertainty indicators can substantially amplify or dampen the impact of global shocks depending on their configuration. This interaction structure helps explain why flexible nonlinear machine-learning models deliver sizeable forecast gains relative to linear benchmarks in Section 4, and it motivates the interconnectedness analysis developed in the next subsection.

4.3 Non-Linearity and Amplification

Figures 4–5 present a unified view of the model’s nonlinear responses to key global drivers across financial, geopolitical, and geo-economic domains. Each panel plots a SHAP dependence curve: the horizontal axis shows the raw feature value, and the vertical axis its Shapley contribution to sovereign risk, separately for five regional clusters (Advanced Economies, Emerging Asia, Emerging Latin America, Emerging Europe, and MENA). The fitted lines are obtained

using a locally weighted LOESS smoother,¹⁴ which traces state-dependent curvature in the marginal effect of each factor by region. Together, these visualizations provide a first look at how different dimensions of global shocks propagate through heterogeneous regional structures.

Figure 4: Global Financial Non-Linearity: SHAP Dependence Plots for Policy Rate and Volatility



Notes: The figure displays SHAP dependence plots for the *Global Policy Rate (FED)* and *Global Financial Volatility (VIX)* across five regional groups—Advanced Economies, Emerging Asia, Latin America, Emerging Europe, and MENA. Each subplot shows the marginal effect of the corresponding variable’s raw value on its SHAP contribution to sovereign risk. The LOESS smoother traces the local curvature of each relationship, capturing nonlinear and state-dependent sensitivities to financial conditions.

- **The global financial block** (FED and VIX) exhibits pronounced convexity and regional asymmetries. Increases in the global policy rate or volatility produce disproportionately large SHAP responses, particularly for Advanced and EM Asia and Latin America, consistent with tightening cycles and risk-off episodes amplifying systemic stress. In contrast, EM Europe shows flatter slopes under moderate conditions but steeper gradients in extreme states, indicating threshold effects in financial transmission. Across all regions, the VIX variable displays robust upward convexity,¹⁵ confirming its role as a dominant amplifier of global risk.
- **The geopolitical-geoeconomic block**, encompassing Geopolitics (GPR) and Economic (EPU) and Trade uncertainty (TPU), displays more complex and region-specific curvature. The GPR variable is flatter for Advanced Economies—indicating limited partial sensitivity to moderate geopolitical tensions—but becomes convex for EM regions, and in particular for EM Europe and MENA, reflecting heightened vulnerability to geopolitical instability in these regions (Caldara and Iacoviello, 2022; Ahir et al., 2018; Baur and Smales, 2024; Fund, 2023b). In terms of geoeconomics, both EPU and TPU exhibit threshold effects: Shapley-value risk responses remain muted under low-to-moderate uncertainty but accelerate sharply beyond critical levels, particularly in Emerging Europe and MENA (Caggiano et al., 2020). These patterns suggest that uncertainty variables act as *latent accelerators* of sovereign risk, activated only during periods of elevated uncertainty or institutional fragility (Fund, 2023a; Pastor and Veronesi, 2021).

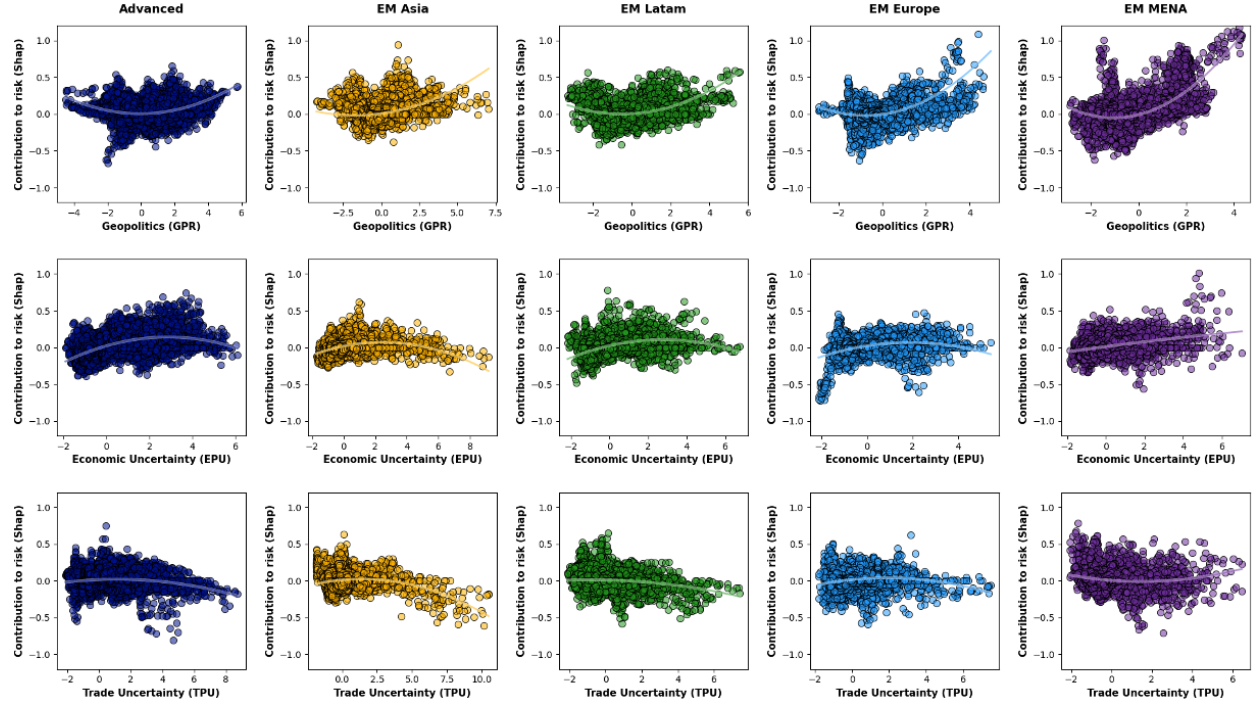
Taken together, the two figures highlight that global shocks propagate through two complementary nonlinear channels: (i) continuous convex amplification via financial markets and (ii) threshold activation via geopolitical and policy uncertainty. The presence of these distinct nonlinearities underscores that sovereign risk is not determined by the linear sum of global factors but by their interaction and regional mediation. The Shapley framework is crucial for uncovering these asymmetries, revealing that the global system’s response to shocks is both *state-dependent* and *region-specific*.

This two-dimensional analysis establishes the empirical foundation for exploring *joint nonlinearities*. The next subsection extends this approach by examining the interaction between pairs of global drivers—mapping their combined

¹⁴ All SHAP dependence plots use a LOESS smoothing fraction of 0.4 with one robust iteration. Both axes are clipped at the 95th percentile to limit the influence of extreme outliers while preserving the overall shape of the nonlinear pattern.

¹⁵ Convexity refers to the nonlinear shape of the model’s partial response—here captured by Shapley values—where the marginal effect of a global factor intensifies at higher levels of the shock, $\partial^2 f(x)/\partial x^2 > 0$. In the plots, this appears as upward-curving SHAP contributions, consistent with state-dependent financial transmission (see Adrian et al., 2022; Bank, 2023; Author, 2024).

Figure 5: Geopolitical and Geoeconomic Non-Linearities: SHAP Dependence Plots for Geopolitics and Economic and Trade Uncertainties



Notes: The figure displays SHAP dependence plots for the *Geopolitical Risk (GPR)*, *Economic Policy Uncertainty (EPU)*, and *Trade Policy Uncertainty (TPU)* indices across five regional groups—Advanced Economies, Emerging Asia, Latin America, Emerging Europe, and MENA. Each subplot shows the marginal effect of the corresponding variable's raw value on its SHAP contribution to sovereign risk. The fitted LOESS curves capture localized nonlinear patterns in the relationship between uncertainty shocks and model predictions.

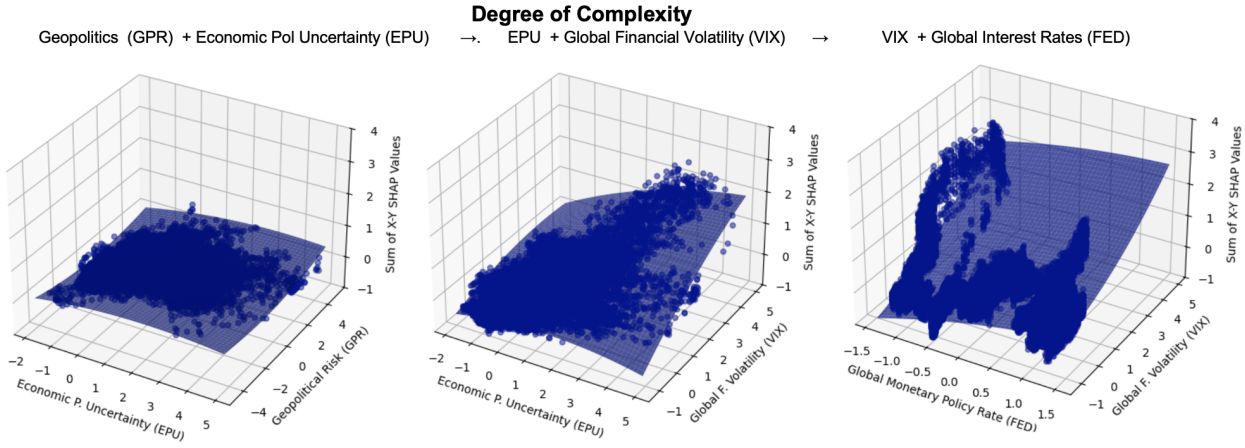
effects through two-dimensional SHAP surfaces—to evaluate how financial, policy, and geopolitical factors jointly shape sovereign risk dynamics.

4.4 State-Dependent Transmission of Shocks

Leveraging the additive property of Shapley values (Lundberg and Lee, 2017), we construct three two-factor scenarios that capture escalating layers of complexity in sovereign risk determination, from localized political and policy uncertainty to global financial tightening. Figure 6 displays the corresponding SHAP dependence plots for Advanced Economies. Appendix D reports analogous dependence graphs for Emerging Markets (Figure 12), which exhibit the same qualitative ranking across scenarios but with steeper and more convex responses, especially in Emerging Europe and MENA.

- *Scenario 1: Geoeconomics and policy uncertainty.* This baseline scenario assesses the combined impact of Geopolitical Risk (GPR) and Economic Policy Uncertainty (EPU). It isolates the effects of non-financial uncertainty, representing the foundational layer of risk stemming from the political and policy-making environment (Baker et al., 2016; Caldara and Iacoviello, 2022).
- *Scenario 2: Uncertainty and financial volatility.* This scenario models an escalation in which policy uncertainty spills over into financial markets. It evaluates the interaction between Economic Policy Uncertainty (EPU) and Global Financial Volatility (VIX), capturing how market sentiment amplifies the risks associated with an unpredictable policy landscape.
- *Scenario 3: Global financial conditions.* The third and most acute scenario represents a comprehensive tightening of global financial conditions. It combines Global Financial Volatility (VIX) with shifts in Global Monetary Policy (FED), illustrating the impact of a simultaneous risk-off shock and a rise in global funding costs, core tenets of the global-financial-cycle literature.

Figure 6: Shapley Contributions by Variable in Advanced Economies: Two-Factor SHAP Dependence Plots



Notes: The figure illustrates the combined impact of key predictors on sovereign CDS spreads for Advanced Economies using two-factor SHAP dependence plots. The bottom row displays the joint influence of Geopolitical Risk (GPR) and Economic Policy Uncertainty (EPU). The middle row plots the joint contribution of EPU and Global Financial Volatility (VIX). The top row shows the joint effect of global financial volatility (VIX) and global monetary policy (FED).

The scenario analysis reveals pronounced nonlinearities and interactions:

Scenario 1: GPR–EPU. For most regions, the combined influence of geopolitical risk and economic policy uncertainty on sovereign CDS spreads is modest. The relatively flat surfaces in the plots indicate low sensitivity to these factors in isolation. However, regional heterogeneity is apparent. The Middle East and North Africa, characterized by structural geopolitical tensions, and, to a lesser extent, Emerging Europe—affected by the Russia–Ukraine conflict—display a more pronounced upward slope, confirming that sovereign risk in these geopolitically sensitive regions is more vulnerable to flare-ups in political and policy-related tensions.

Scenario 2: EPU–VIX. When economic policy uncertainty is combined with a rise in global volatility, the impact on sovereign risk increases sharply. This aligns with theories of uncertainty shocks, which posit that their effects are magnified under conditions of financial stress (Bloom, 2009). The steeper surfaces in the plots illustrate a strong positive interaction: high economic policy uncertainty in a high-VIX environment is substantially more detrimental than either shock occurring alone.

Scenario 3: VIX–FED. A simultaneous spike in global volatility and a tightening of global monetary policy leads to the largest and most nonlinear increases in sovereign risk. This captures the essence of the global financial cycle, where U.S. monetary policy and global risk aversion act as dominant “push” factors for international capital flows and risk premia. The surfaces also show that the impact of a volatility shock can be partially contained when interest rates remain low, but this mitigating effect is weaker than the amplification that occurs when both factors rise in tandem. The response to volatility is markedly state-dependent (Bekaert et al., 2013): it is powerfully amplified when monetary policy is tight (Rey, 2013; Miranda-Agrippino and Rey, 2020) and partially contained when policy is accommodative, for instance through the risk-taking channel (Bruno and Shin, 2015; Miranda-Agrippino and Rey, 2020).

In summary, the scenarios reveal a critical transmission channel. *Geoeconomic or policy uncertainty, while often manageable in isolation, becomes a potent threat when it coincides with elevated global volatility and tighter financial conditions.* The interaction between these domains is paramount in determining sovereign vulnerability, especially in Emerging Markets.

4.5 Interconnectedness and Network Dynamics

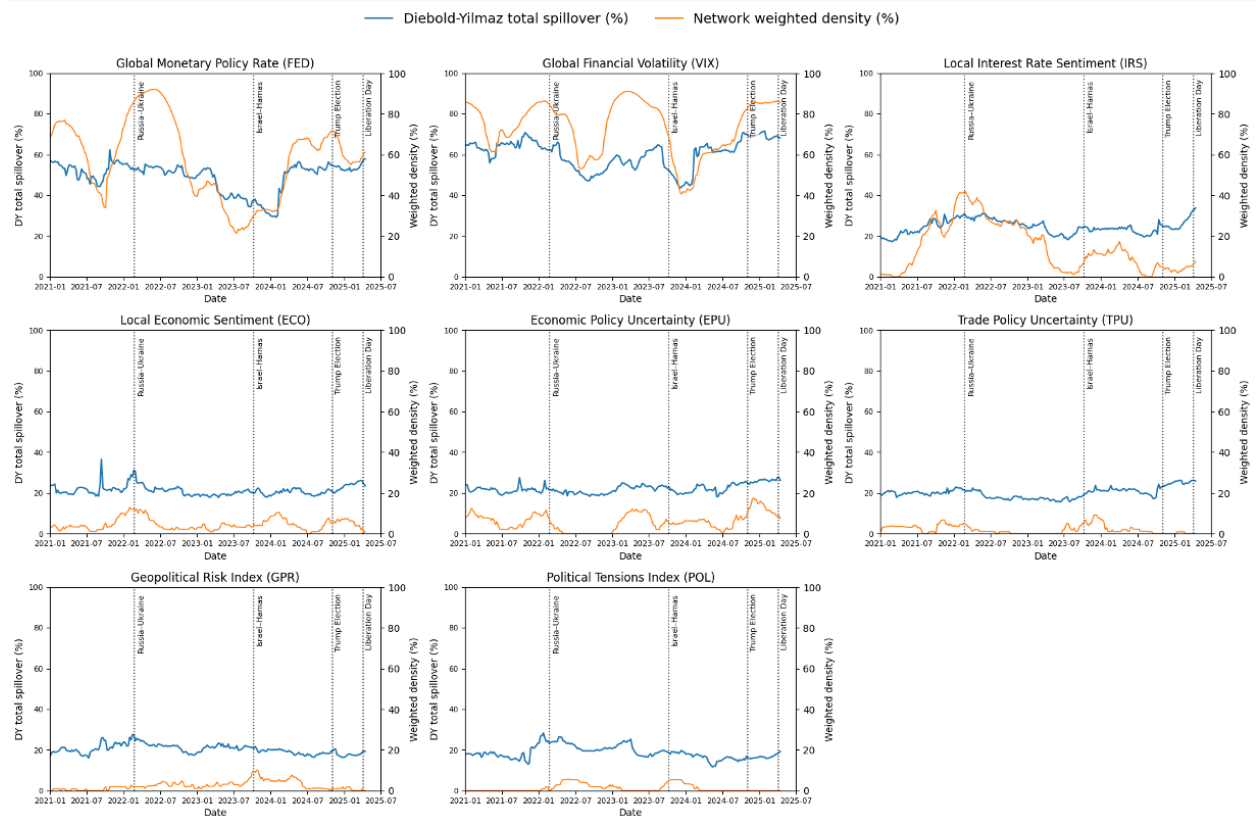
To assess how sovereign-risk attributions co-move and propagate across countries, we construct two complementary interconnectedness measures from the daily, country-level Shapley-implied risk series. First, we compute a Diebold–Yilmaz dynamic spillover index based on rolling VARs, which summarizes the extent of directional, lagged transmission of shocks across countries. Second, we construct a non-parametric weighted network-density index from thresholded Spearman correlations, capturing contemporaneous clustering in sovereign-risk attributions. Full details on rolling-

window construction, VAR estimation, lag selection, generalized forecast-error variance decomposition (GFEVD) normalization, and density computation are provided in Appendix C.

Taken together, the two measures map distinct propagation mechanisms. High spillovers in the Diebold–Yilmaz index indicate multi-country transmission through lagged channels; high density reflects synchronous co-movement driven by common shocks. Episodes where both rise simultaneously correspond to periods of systemic stress and broad-based global repricing. Conversely, high density but low spillovers denotes localized synchronization without contagion, whereas high spillovers alongside low density indicate directional but unsynchronized propagation.

Figure 7 displays dynamic networks in the *Shapley attribution space* using these two indices: the Diebold–Yilmaz (DY) total spillover index (blue line) and the weighted network density (orange line). Equalized vertical scales allow direct comparisons across variables and permit a clearer assessment of transmission hierarchies. Each panel tracks cross-country interconnectedness from 2021 onward, with vertical markers for the Russia–Ukraine invasion (February 2022), the Hamas–Israel conflict (October 2023), and the 2024 U.S. election. Interpreted jointly, DY captures directional propagation, while density reflects synchronous co-movement. Their combined dynamics help distinguish between system-wide stress, common but short-lived shocks, and narrower propagation through specific channels. Three main patterns emerge:

Figure 7: Diebold–Yilmaz Spillovers and Network Density (2021–2025)



Notes: The figure reports dynamic spillover effects (blue line) and network density (orange line) for sovereign-risk determinants. Top row: global financial drivers (2-year UST, VIX, local interest rate sentiment). Middle row: local economic sentiment and uncertainty indices (EPU, TPU). Bottom row: geopolitical risk (GPR) and political tensions (POL). All indices are computed from daily, country-level Shapley attributions.

- *Global financial conditions are the dominant and persistent transmitters.* The global monetary policy rate (FED) and global financial volatility (VIX) display the highest and most sustained DY values across the sample. Both spike sharply in early 2022, normalize through mid-2023, and rise again into late 2024. Network density moves closely with DY, consistent with episodes of system-wide repricing rather than localized contagion. With

common vertical scales across panels, the primacy of global rates and volatility as cross-country transmission hubs becomes clear, echoing their dominant Shapley contributions and interaction effects documented above.

- *Local macro sentiment transmits directionally but with limited persistence.* Local interest rate sentiment (INT) shows pronounced DY increases in 2022, coinciding with the global tightening–volatility shock, but density remains comparatively subdued thereafter. This combination—moderate DY with low density—indicates directional propagation through monetary channels without broad synchronization. Local economic sentiment (ECO) displays a gradual DY rise into 2024–2025, but density remains intermittent, pointing to slow diffusion rather than unified contagion.
- *Geopolitical and policy-uncertainty shocks are episodic and synchronous.* Geopolitical risk (GPR) and political tensions (POL) generate short, sharp density spikes around October 2023 during the Hamas–Israel conflict, while DY remains muted—an archetypal “common news” shock. Economic policy uncertainty (EPU) and, intermittently, trade policy uncertainty (TPU) show similar brief increases. By late 2024, however, EPU displays rising density and DY, indicative of a broader policy-uncertainty cycle around the U.S. election rather than a region-specific disturbance. TPU remains consistently secondary, with only isolated upticks.

Taken together, the dual-metric evidence establishes a clear hierarchy of transmission channels and links back to the Shapley results. Episodes with *simultaneously high density and high DY*—such as the early-2022 surge in global rates and volatility around the Russia–Ukraine invasion—reflect systemic stress, when shocks both synchronize markets and propagate dynamically across borders. By contrast, *high density with low DY*, exemplified by the October 2023 Hamas–Israel conflict, captures common news events that trigger widespread repricing without durable contagion. Finally, *moderate DY with low density*, observed in the run-up to the 2024 U.S. election as policy uncertainty increased, corresponds to directional spillovers through policy channels without full synchronization of global markets.

The overarching pattern is that global financial conditions—interest rates and volatility—anchor the baseline level of interconnectedness, ensuring that shocks in these domains reverberate more broadly and persistently than domestic or geopolitical developments. Geopolitical and policy-related uncertainty, while capable of generating sharp co-movements, tend to act as episodic amplifiers whose effects dissipate unless reinforced by global financial tightening. The hierarchy is therefore clear: global financial shocks set the systemic baseline, domestic uncertainty transmits through narrower channels, and geopolitical events typically produce short-lived synchronization without sustained contagion.

5 Narrative Analysis of Crisis Episodes

This section uses the Shapley-based decomposition to study three recent episodes that differ in scope and transmission: an interstate war (Russia–Ukraine), a localized conflict (Hamas–Israel), and a geoeconomic trade shock (U.S. tariffs). For each case, we feed the realized data through the frozen machine-learning model and track daily Shapley contributions for the relevant countries. By virtue of *local accuracy* and *consistency*, Shapley values decompose day-by-day changes in model-predicted sovereign risk into positive and negative contributions by each driver, allowing us to trace transmission channels in a way that is directly comparable across episodes.

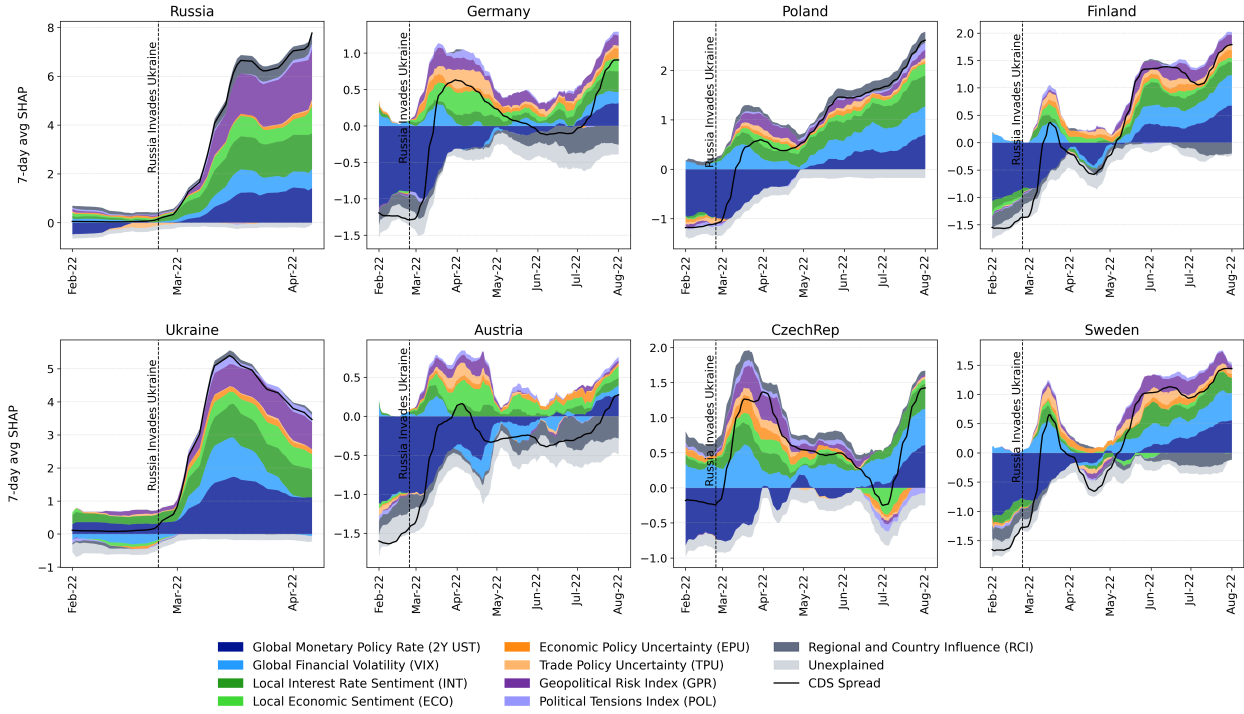
Taken together, these case studies provide concrete illustrations of the patterns documented in the Shapley relevance, nonlinear, and network analysis. The Russia–Ukraine war corresponds to a systemic stress episode, with high density and spillovers in the Shapley attribution space. The Hamas–Israel conflict exemplifies a localized common shock with limited cross-country contagion. The U.S. tariff conflict is a geoeconomic shock transmitted both through trade partners and via the global financial channel.

5.1 Geopolitical Shock: The Russia–Ukraine War

The February 24, 2022 invasion illustrates how a regional conflict can evolve into a systemic macro-financial shock. Figure 8 shows that sovereign spreads for the direct combatants (Russia and Ukraine) spiked sharply. For Russia, the surge reflects not only Geopolitical Risk (GPR) but also a rapid deterioration in domestic conditions and, subsequently, tighter global financial conditions. Sanctions and market exclusion magnified these pressures, consistent with evidence that conflict episodes raise sovereign spreads and volatility (Caldara and Iacoviello, 2022; Boubaker et al., 2023). For Ukraine, spreads increased immediately as geopolitical premia combined with broad-based declines in domestic conditions and heightened policy uncertainty, in line with historical findings on war shocks (Caldara and Iacoviello, 2022).

Among European neighbors, GPR rises broadly but more moderately; Economic Policy Uncertainty (EPU) and Trade Policy Uncertainty (TPU) also increase, reflecting proximity and energy dependence. The most salient dynamic in the Shapley decompositions is the swift deterioration first in global policy rates and then in global financial volatility.

Figure 8: Shapley contribution changes to sovereign risk after the Russian invasion of Ukraine



Notes: The figure plots the evolution of Shapley contributions to sovereign CDS spreads for selected countries before and after February 2022. For Russia and Ukraine, contributions from global drivers (global monetary policy rates, global financial volatility) and geopolitical risk measures surge. For European economies (Germany, Poland, Finland, Austria, Czech Republic, Sweden), the impact is more moderate but still material, with local sentiment and policy uncertainty amplifying exposure. Global financial conditions remain the dominant explanatory factor, while geopolitical and political tensions add substantial power for directly exposed countries.

Major central banks (including the Federal Reserve and the ECB) pivoted from accommodation to tightening roughly three months after the shock, lifting funding costs and depressing risk appetite. The initial spike in GPR is thus quickly overshadowed in the attributions by rising policy uncertainty and, in many cases, by the stronger influence of global monetary policy. Reliance on Russian energy and supply-chain disruptions amplified the inflation and uncertainty channels, transforming the geopolitical shock into a broader macro-financial one once central banks reacted to the inflation impulse (Novta and Pugacheva, 2021). According to ECB officials, “the Russian invasion of Ukraine in February 2022 was a distinct additional shock that accounted for most of the extraordinary surge in inflation during 2022, especially in Europe” (Lane, 2024). Given the nonlinear nature of inflation dynamics, this implies the war was pivotal in turning already elevated post-pandemic pressures into an “extraordinary surge.”

Taken together, the evidence reveals a cascade:

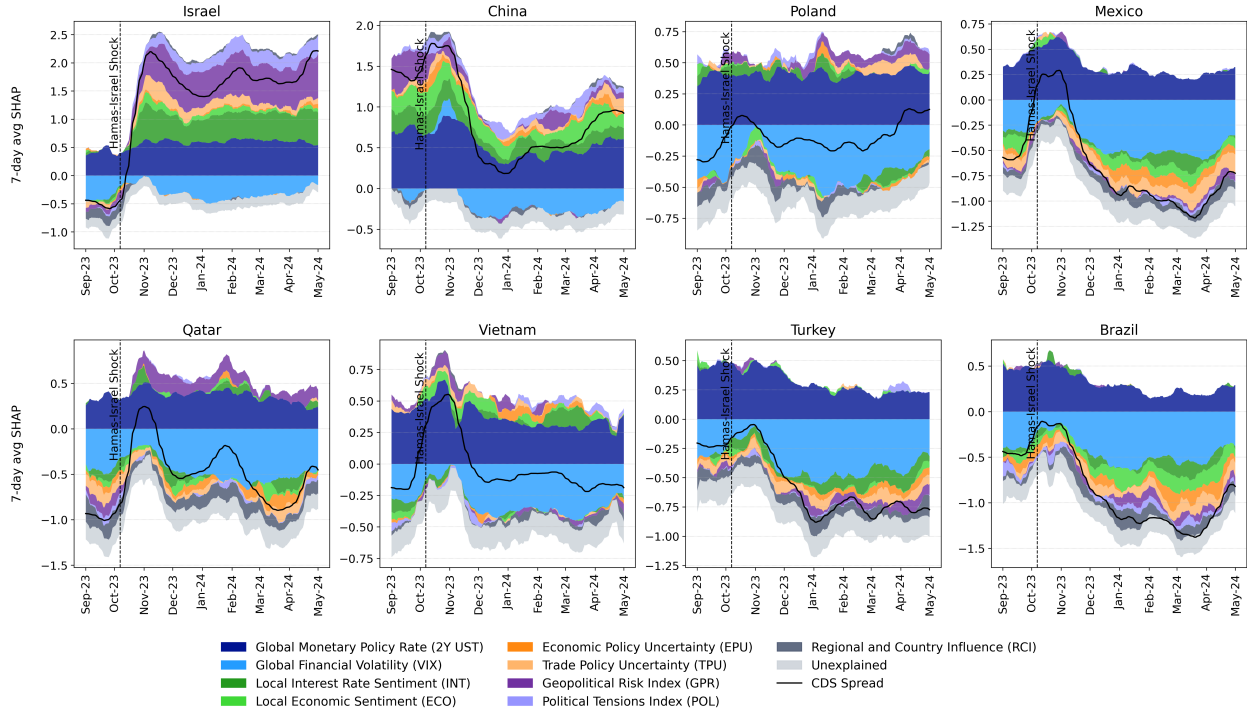
geopolitical shock \Rightarrow commodity and inflation shock \Rightarrow policy uncertainty \Rightarrow global financial tightening.

In terms of the broader results, this episode is a textbook case in which a regional conflict is transformed into systemic geoeconomic stress once it interacts with the global financial cycle (Bloom, 2009; Rey, 2013; Aiyar et al., 2023).

5.2 Geopolitical Shock: The Hamas–Israel Conflict

By contrast, the October 2023 Hamas–Israel conflict was a more localized geopolitical shock. Figure 9 shows that for Israel the effect was immediate and persistent, driven primarily by geopolitical factors alongside weakening domestic conditions and rising policy and trade uncertainty, consistent with conflict risk being priced directly in the affected sovereign (Caldara and Iacoviello, 2022). Neighboring economies (e.g., Qatar, Turkey) experienced muted increases in geopolitical contributions, indicating contained regional spillovers. For most other Emerging Markets (e.g., Mexico, Brazil, Poland) and major Asian economies (e.g., China, Vietnam), GPR remained essentially flat in the Shapley decompositions, underscoring the limited systemic reach (Novta and Pugacheva, 2021).

Figure 9: Shapley contribution changes to sovereign risk after the Hamas–Israel conflict



Notes: The figure plots Shapley contributions to sovereign CDS spreads after October 2023. For Israel, geopolitical risk and political tensions dominate, with heightened global volatility. Qatar and Turkey show increases in geopolitical and political contributions but remain secondary to global drivers. For non-regional economies (China, Vietnam, Mexico, Poland, Brazil), global financial conditions (monetary policy, volatility) remain primary; geopolitical spillovers are limited.

Crucially, the conflict coincided with signals that the global tightening cycle was ending.¹⁶ As policy-rate expectations softened and volatility receded, global financial conditions shifted from amplifying sovereign risk to supporting a broad-based decline in premia, offsetting contagion outside the region. In terms of our interconnectedness measures, this corresponds to high density but low spillovers: a common news shock that is largely absorbed by a benign global financial backdrop (Rey, 2013; Bloom, 2009).

5.3 Geoeconomic Fragmentation: Trump Election and U.S. Tariffs

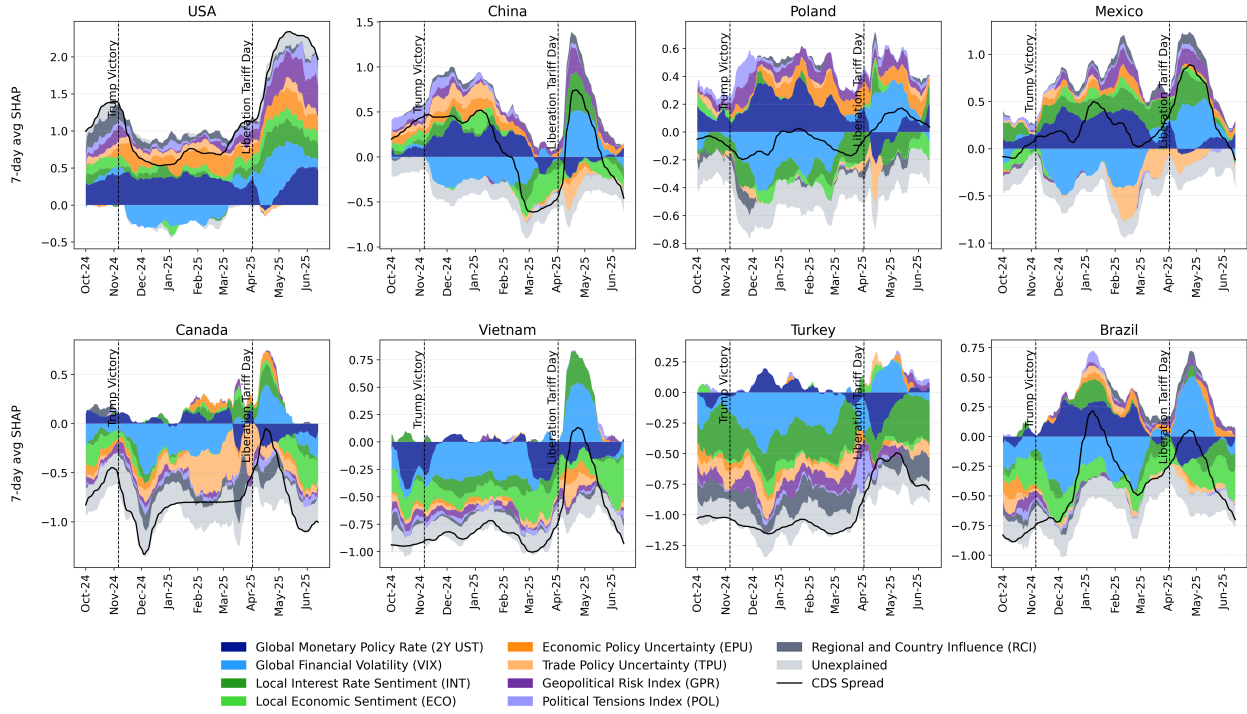
The 2024 U.S. presidential election and subsequent tariff measures constitute a geoeconomic shock transmitted through trade and policy uncertainty. The response in the Shapley attributions unfolds in two phases: the election in November 2024 and the tariff implementation in early 2025 (“Liberation Day,” April 2, 2025). Initially, EPU and TPU contributions spike in the United States and key trading partners (Canada, Mexico, China), reflecting heightened policy unpredictability.¹⁷ For many other Emerging Markets, immediate effects are more muted and transmitted primarily via global uncertainty. Some countries (e.g., Mexico) also see geopolitical contributions rise, reflecting concurrent rhetoric on immigration and security; China and Poland show modest GPR deterioration as well.

With tariff announcements and implementation, uncertainty crystallizes into a concrete geoeconomic shock. For the United States, China, Mexico, and Canada, EPU and TPU contributions become dominant drivers of sovereign risk, consistent with evidence that protectionism and sanctions destabilize credit premia (Ahn and Ludema, 2020; Itskhoki and Ribakova, 2024). For other EMs (e.g., Poland, Turkey, Brazil, Vietnam), effects are indirect: tariffs raise global volatility and alter monetary expectations, transmitting risk through the global financial channel rather than direct trade exposure (Glick and Rose, 1999; Diebold and Yilmaz, 2012).

¹⁶By October 2023, the Federal Reserve had held the funds rate at 5.25–5.50% since July and noted in its 2023 Monetary Policy Report that policy was “likely at its peak for this tightening cycle” Board of Governors of the Federal Reserve (2023). The September 2023 FOMC minutes also emphasized caution and data dependence Board Governors of Federal Reserve (2023).

¹⁷Implementation was erratic: a sweeping 25% tariff threat on all imports from Canada and Mexico (1 February 2025) was quickly amended to exempt USMCA-compliant sectors (e.g., autos), highlighting policy volatility.

Figure 10: Shapley contribution changes to sovereign risk after the U.S. election and tariff policy



Notes: The figure shows Shapley contribution dynamics around the 2024 U.S. election and subsequent tariff announcements. For the United States, sovereign risk increases after the election and accelerates with tariff measures, driven by TPU, EPU, and global volatility. Spillovers are evident in Mexico, Canada, China, and Brazil through trade and policy uncertainty. For other economies (Poland, Turkey, Vietnam), global financial drivers remain central, with uncertainty effects rising around tariff dates. The evidence supports dual transmission: direct trade exposure for core participants and broader amplification through global financial volatility.

In sum, this episode exemplifies a geoeconomic scenario: policy uncertainty materializes as tariffs, reshaping sovereign risk both directly (via trade exposure) and indirectly (via global financial conditions). In the language of our earlier results, it combines a shock to the geoeconomic block (EPU/TPU) with an endogenous shift in the global financial block (FED/VIX), reinforcing the nonlinear interaction patterns documented in the SHAP dependence plots.

5.4 Comparing the Three Episodes

Taken together, the three cases reveal systematic differences in shock type, transmission, and interaction with the global financial cycle:

- *Nature of the shock.* Russia–Ukraine and Hamas–Israel are geopolitical shocks dominated by GPR; both show country-level deteriorations in domestic conditions and uncertainty for directly affected sovereigns, consistent with recent evidence on household and firm responses to geopolitical risk (Gorodnichenko et al., 2025).¹⁸ The tariff episode is geoeconomic, driven largely by EPU/TPU and prospective policy responses to the inflationary effects of trade restrictions.
- *Primary transmission channel.* Russia–Ukraine propagated via *proximity* and then via *energy and inflation* into broader macro-financial stress. Hamas–Israel remained largely regional, with the global footprint transmitted mainly through the *global financial channel* (VIX, policy expectations) in an easing environment. Tariffs propagated through a *direct trade channel* for the United States and core partners, while raising volatility and shifting monetary expectations for others.
- *Nonlinear interaction with the global financial cycle (rates and volatility).* Global conditions were decisive but state-dependent. In Russia–Ukraine, the war exacerbated an ongoing inflation impulse, prompting aggressive

¹⁸Gorodnichenko et al. (2025) document that higher perceived conflict durations raise expectations of stagflation, worsen views on public finances and household conditions, and depress consumption, complementing evidence on adverse firm outcomes.

tightening. In Hamas–Israel, a dovish pivot offset broader contagion. In the tariff case, the trade shock itself triggered tighter global financial conditions by raising volatility and altering policy-rate expectations. These patterns align with the primacy of the global financial cycle (Rey, 2013) and the amplification of uncertainty under financial stress (Bloom, 2009).

Overall, the global impact of shocks depends critically on their interaction with the global financial cycle, which governs whether effects are amplified, muted, or offset. The narrative evidence is fully consistent with the model-based findings: global financial factors dominate average Shapley contributions and network spillovers, while geopolitical and geoeconomic shocks matter most when they coincide with tight and volatile global conditions, in line with the nonlinear amplification patterns documented in Section 4.

6 Conclusion

This study shows that sovereign risk is shaped by a complex interaction between global financial conditions, domestic sentiment, and geopolitical or policy-related uncertainty. Using a high-frequency panel for 42 advanced and emerging economies and a broad set of machine-learning models, we find that *non-linear methods—particularly tree-based ensembles—substantially outperform linear benchmarks in predicting sovereign CDS spreads*. This underscores the importance of accounting for threshold effects, asymmetries, and state dependence in sovereign-risk dynamics.

Text-based indicators capture dimensions of sovereign risk that are not fully reflected in contemporaneous financial variables, and their predictive value is inherently non-linear. The gains from adding news variables are modest in linear models but become sizeable once the specification allows for interactions and non-linearities. In other words, *the value of news depends not only on which indicators are included, but on how they are integrated*. Model choice is therefore central to exploiting high-frequency, unstructured information for sovereign-risk assessment.

Having validated the predictive power of our preferred model out-of-sample, we turn to an in-sample narrative analysis based on Shapley value decompositions. This reveals a clear hierarchy of drivers. *Global monetary policy and global financial volatility emerge as dominant “push” factors*, consistent with the global financial cycle literature. Domestic macro-financial sentiment helps explain cross-country dispersion in spreads, while geopolitical risk and policy uncertainty act primarily as non-linear amplifiers whose effects become sizeable when global conditions tighten. Scenario exercises show that uncertainty shocks in isolation have moderate effects, but when combined with adverse global financial conditions they produce powerful non-linear amplifications of sovereign risk.

We also provide a joint view of cross-country interconnectedness by combining Diebold–Yilmaz spillover indices with a network-based density measure computed in the space of Shapley attributions. *Global financial variables—the U.S. two-year yield and the VIX—emerge as persistent propagation hubs*, generating both directional spillovers and broad co-movements. Local macro sentiment amplifies shocks during stress episodes but tends to decouple as conditions normalize, while geopolitical and policy-uncertainty shocks generate sharp but episodic co-movements with limited sustained transmission. This hierarchy helps distinguish systemic episodes, in which both spillovers and density rise together, from more localized events that mainly generate short-lived synchronization.

Finally, we document pronounced heterogeneity across regions and asset classes. Advanced economies are especially sensitive to shifts in global monetary policy, while emerging markets—particularly in Latin America and Asia—exhibit heightened exposure to global volatility. Geopolitical risk is most salient in Emerging Europe and the Middle East and North Africa, where structural and institutional vulnerabilities magnify the impact of conflict and political tensions. *Case studies of the Russia–Ukraine war, the Hamas–Israel conflict, and recent U.S. tariff hikes illustrate these mechanisms in real time*, corresponding respectively to episodes of systemic stress, localized common shocks, and geoeconomic trade shocks.

Taken together, our findings suggest that sovereign risk cannot be understood in a purely global or purely domestic framework. Instead, it reflects the interaction between global financial conditions, regional and institutional characteristics, and news shocks that operate through non-linear and state-dependent channels. For policymakers, this implies that vulnerability management depends as much on external financial conditions as on domestic fundamentals, and that monitoring high-frequency text-based indicators can provide timely warnings when uncertainty or geopolitical risks begin to amplify the effects of global tightening. For researchers, a natural next step is to embed these non-linear, news-driven transmission channels into structural models of sovereign risk and capital allocation, and to test whether similar mechanisms arise for other asset classes, maturities, and currencies.

Beyond these substantive results, the paper also carries a methodological message. By designing a strictly pseudo-real-time evaluation with buffers around moving-average windows, we show that *careful attention to data leakage and forecast design can materially affect the ranking of models and the measured value of news*. Our use of Shapley-based decompositions further illustrates how flexible machine-learning tools can be combined with interpretable diagnostics

to bridge the gap between prediction and narrative analysis. Together, these elements point toward a research agenda in which high-frequency news indicators, non-linear forecasting tools, and transparent model-attribution methods are jointly used to strengthen sovereign-risk surveillance and early-warning systems.

References

Acemoglu, D., Ozdaglar, A., and Tahbaz-Salehi, A. (2015). Systemic risk and stability in financial networks. *American Economic Review*, 105(2):564–608. Citation key matches text; authors corrected from Duffie/Eisenberg to Acemoglu et al. based on title.

Adrian, T., Duarte, F., and Natalucci, F. (2022). A new era of global financial vulnerability. *International Monetary Fund. Global Financial Stability Report*. International Monetary Fund.

Ahir, H., Bloom, N., and Furceri, D. (2018). The world uncertainty index. *Brookings Papers on Economic Activity*, pages 343–400.

Ahn, D. P. and Ludema, R. D. (2020). The sword and the shield: The economics of targeted sanctions. *European Economic Review*, 130:103578.

Aiyar, S., Presbitero, A. F., and Ruta, M. (2023). Geoeconomic fragmentation and the future of multilateralism. International Monetary fund. Staff Discussion Note SDN/2023/001, International Monetary Fund.

Alter, A. and Beyer, A. (2014). The dynamics of spillover effects during the european sovereign debt turmoil. *Journal of Banking & Finance*, 42:134–153.

Athey, S. (2018). The impact of machine learning on economics. *The Economics of Artificial Intelligence: An Agenda*, pages 507–547.

Athey, S. and Imbens, G. W. (2019). Machine learning methods that economists should know about. *Annual Review of Economics*, 11:685–725.

Author, A. (2024). Quantile vix and global financial risk. *Borsa Istanbul Review*.

Bahaj, S. and Reis, R. (2022). Central banking in challenging times: Central bank liquidity lines. *American Economic Journal: Macroeconomics*, 14(2):110–150.

Baker, S. R., Bloom, N., and Davis, S. J. (2016). Measuring economic policy uncertainty. *The Quarterly Journal of Economics*, 131(4):1593–1636.

Bank, E. C. (2023). European central bank working paper no. 2973. Technical report, European Central Bank.

Bank for International Settlements (2022). Bis annual economic report 2022. Technical report, Bank for International Settlements.

Barabási, A.-L. (2016). *Network Science*. Cambridge University Press, Cambridge.

Battiston, S., Caldarelli, G., et al. (2016). The price of complexity in financial networks. *Proceedings of the National Academy of Sciences*, 113(36):10031–10036.

Baur, D. G. and Smales, L. A. (2024). Flight-to-quality – money market mutual funds and stablecoins during the march 2023 banking crisis. *Economics Letters*, 234:Article 111464.

Bekaert, G., Hoerova, M., and Lo Duca, M. (2013). Risk, uncertainty and monetary policy. *Journal of Monetary Economics*, 60(7):771–788.

Benchimol, J. and Palumbo, L. (2024). Sanctions and russian online prices. *Journal of Economic Behavior & Organization*, 225:483–521.

Bloom, N. (2009). The impact of uncertainty shocks. *Econometrica*, 77(3):623–685.

Bluwstein, K., Buckmann, M., Kapadia, S., and Stockdale, O. (2023). Systemic risk and financial spillovers: A machine learning approach. *Journal of Monetary Economics*, 134:80–99.

Board Governors of Federal Reserve (2023). Minutes of the federal open market committee, september 2023. Minutes, Board of Governors of the Federal Reserve System, Washington, DC. 2023b.

Board of Governors of the Federal Reserve (2023). Monetary policy report. Report, Board of Governors of the Federal Reserve System, Washington, DC. 2023a.

Bondarenko, Y., Lewis, V., Rottner, M., and Schüler, Y. (2024). Geopolitical risk perceptions. *Journal of International Economics*, 152:104005.

Boubaker, S., Goodell, J. W., Kumar, S., and Sureka, R. (2023). Geopolitical risk and energy stock performance: Evidence from the Russia–Ukraine conflict. *Journal of Commodity Markets*, 30:100325.

Breiman, L. (2001). Random forests. *Machine Learning*, 45(1):5–32.

Broner, F. and Varela, L. (2017). Reversal of capital flows and emerging market vulnerability. *Journal of Monetary Economics*, 85:28–44.

Bruno, V. and Shin, H. S. (2015). Capital flows and the risk-taking channel of monetary policy. *Journal of Monetary Economics*, 71:119–132.

Caggiano, G., Castelnuovo, E., and Figueres, J. (2020). Economic policy uncertainty spillovers in booms and busts. *Journal of Monetary Economics*, 115:735–751.

Caldara, D. and Iacoviello, M. (2022). Measuring geopolitical risk. *American Economic Review*, 112(4):1194–1225.

Caldara, D., Iacoviello, M., Molligo, P., Prestipino, A., and Raffo, A. (2020). The economic effects of trade policy uncertainty. *Journal of Monetary Economics*, 109:38–59.

Calvo, G. A., Izquierdo, A., and Mejía, L.-F. (2004). On the empirics of sudden stops: The relevance of balance-sheet effects. *NBER Working Paper*, 10520.

Calvo, G. A., Leiderman, L., and Reinhart, C. M. (1996). Inflows of capital to developing countries in the 1990s. *Journal of Economic Perspectives*, 10(2):123–139.

Clayton, C., Coppola, A., Maggiori, M., and Schreger, J. (2025). Geoeconomic pressure. Working Paper 34020, National Bureau of Economic Research.

Cont, R. (2001). Empirical properties of asset returns: stylized facts and statistical issues. *Quantitative Finance*, 1(2):223–236.

Davis, S. J., Hansen, S., and Seminario-Amez, C. (2025a). Macro shocks and firm-level response heterogeneity. Working Paper.

Davis, S. J., Hansen, S., and Seminario-Amez, C. (2025b). Macro shocks and firm-level response heterogeneity. Working Paper.

Didier, T., Hevia, C., and Schmukler, S. L. (2012). Financial globalization in emerging economies: Much ado about nothing? *Journal of Development Economics*, 98(1):86–104.

Diebold, F. X. and Yilmaz, K. (2012). Better to give than to receive: Predictive directional measurement of volatility spillovers. *International Journal of Forecasting*, 28(1):57–66.

Diebold, F. X. and Yilmaz, K. (2014). On the network topology of variance decompositions: Measuring the connectedness of financial firms. *Journal of Econometrics*, 182(1):119–134.

Du, W., Im, J., and Schreger, J. (2018a). The dollar, bank funding and global financial conditions. *Journal of Finance*, 73(2):537–586.

Du, W., Im, J., and Schreger, J. (2018b). The dollar, bank funding and global financial conditions. *The Journal of Finance*, 73(2):537–586.

Eichengreen, B., Hausmann, R., and Panizza, U. (2021a). Original sin redux: A modern assessment of emerging-market vulnerabilities. *Journal of International Money and Finance*, 110:102280.

Eichengreen, B., Mody, A., Nedeljkovic, M., and Sarno, L. (2021b). How global financial cycles and domestic fundamentals interact. *Journal of International Economics*, 132:103509.

Fernández, A., González, A., and Rodríguez, D. (2018). Commodity price synchronicity and financial variables. *Journal of International Financial Markets, Institutions and Money*, 56:26–40.

Fernández-Villaverde, J., Li, Y., Xu, L., and Zanetti, F. (2025). Charting the uncharted: The (un)intended consequences of oil sanctions and dark shipping. Working Paper 33486, National Bureau of Economic Research.

Fernández-Villaverde, J., Mineyama, T., and Song, D. (2024a). Are we fragmented yet? measuring geopolitical fragmentation and its causal effects. Working Paper 32638, National Bureau of Economic Research.

Fernández-Villaverde, J., Mineyama, T., and Song, D. (2024b). Are we fragmented yet? measuring geopolitical fragmentation and its causal effects. Working Paper 32638, National Bureau of Economic Research.

Fratzscher, M. (2012). Capital flows, push versus pull factors and the global financial crisis. *Journal of International Economics*, 88(2):341–356.

Friedman, J. H. (2001). Greedy function approximation: A gradient boosting machine. *Annals of Statistics*, 29(5):1189–1232.

Fund, I. M. (2023a). Global financial stability report. International Monetary Fund, April 2023.

Fund, I. M. (2023b). Regional economic outlook: Middle east and central asia. International Monetary Fund, Washington, DC.

Gelos, R. G., Sahay, R., and Sandleris, G. (2011). Sovereign borrowing by developing countries: What determines the bond spread? *Journal of Development Economics*, 96(2):273–282.

Gentzkow, M., Kelly, B., and Taddy, M. (2019). Text as data. *Journal of Economic Literature*, 57(3):535–574.

Glick, R. and Rose, A. K. (1999). Contagion and trade: why are currency crises regional? *Journal of International Money and Finance*, 18(4):603–617.

Goldberg, L. and Cetorelli, N. (2020a). Banking globalization, monetary transmission, and the global financial cycle. *Journal of International Economics*, 125:103–118.

Goldberg, L. S. and Cetorelli, N. (2020b). Banking globalization, monetary transmission, and the global financial cycle. *Journal of International Economics*, 125:103–118.

Gopinath, G., Boz, E., Casas, C., Díez, F. J., Gourinchas, P.-O., and Plagborg-Møller, M. (2020). Dominant currency paradigm. *American Economic Review*, 110(3):677–719.

Gorodnichenko, Y., Georgarakos, D., Kenny, G., and Coibion, O. (2025). The impact of geopolitical risk on consumer expectations and spending. Working Paper 34195, National Bureau of Economic Research.

Goulet Coulombe, P., Leroux, M., Stevanovic, D., and Surprenant, S. (2022). How is machine learning useful for macroeconomic forecasting? *Journal of Applied Econometrics*, 37(5):920–964.

Gu, S., Kelly, B. T., and Xiu, D. (2020). Empirical asset pricing via machine learning. *The Review of Financial Studies*, 33(5):2223–2273.

Hale, G., Kapan, T., and Minoiu, C. (2020a). Bank networks and cross-border financial transmission. *Journal of International Economics*, 124:103127.

Hale, G., Kapan, T., and Minoiu, C. (2020b). Bank networks and cross-border financial transmission. *Journal of International Economics*, 124:103–127.

Hamilton, J. D. (1989). A new approach to the economic analysis of nonstationary time series and the business cycle. *Econometrica*, 57(2):357–384.

Hassan, T. A., Hollander, S., van Lent, L., and Tahoun, A. (2019). Firm-level political risk: Measurement and effects. *The Quarterly Journal of Economics*, 134(4):2135–2202.

Hastie, T., Tibshirani, R., and Friedman, J. (2009). *The Elements of Statistical Learning: Data Mining, Inference, and Prediction*. Springer Series in Statistics. Springer, New York, 2nd edition.

Hoerl, A. E. and Kennard, R. W. (1970). Ridge regression: Biased estimation for nonorthogonal problems. *Technometrics*, 12(1):55–67.

International Monetary Fund (2022). Global financial stability report. Technical report, International Monetary Fund.

Itskhoki, O. and Ribakova, E. (2024). The economics of sanctions: From theory into practice. Technical report, Brookings Institution. Brookings Papers on Economic Activity Conference Draft.

Jolliffe, I. T. (2002). *Principal Component Analysis*. Springer Series in Statistics. Springer, New York, 2nd edition.

Joseph, A. and Strobel, F. (2021). Machine learning for financial crises prediction: An empirical comparison with linear models. *Journal of Financial Stability*, 56:100939.

Koenker, R. and Bassett, G. (1978). Regression quantiles. *Econometrica*, 46(1):33–50.

Lane, P. R. (2024). European central bank monetary policy and the inflation surge. *European Central Bank Economic Bulletin*. Available at: https://www.ecb.europa.eu/pub/economic-bulletin/articles/2024/html/ecb_ebart202402_01~d1f7f8e8b6.en.html.

LeCun, Y., Bengio, Y., and Hinton, G. (2015). Deep learning. *Nature*, 521(7553):436–444.

Leetaru, K. and Schrot, P. A. (2013). Gdelt: Global data on events, location, and tone, 1979–2012. Technical Report Version 1.0, GDELT Project. Presented at the International Studies Association Annual Convention, San Francisco, CA.

Lundberg, S. M. and Lee, S.-I. (2017). A unified approach to interpreting model predictions. In *Advances in Neural Information Processing Systems*, volume 30, pages 4765–4774. Curran Associates, Inc.

Maggiori, M., Neiman, B., and Schreger, J. (2020). International currencies and capital allocation. *Journal of Political Economy*, 128(6):2019–2066.

Manela, A. and Moreira, A. (2017). News implied volatility and disaster concerns. *Journal of Financial Economics*, 123(1):137–162.

Miranda-Agrippino, S. T. and Rey, H. (2020). U.s monetary policy and the global financial cycle. *Review of Economic Studies*, 87(6):2754–2776.

Molnar, C. (2019). *Interpretable Machine Learning*. Lulu.com.

Mueller, H. and Rauh, C. (2018). Reading between the lines: Prediction of political violence using newspaper text. *American Political Science Review*, 112(2):358–375.

Mueller, H. and Rauh, C. (2022). Using past violence and current news to predict changes in violence. *International Interactions*, 48(4):579–596.

Mullainathan, S. and Spiess, J. (2017). Machine learning: An applied econometric approach. *Journal of Economic Perspectives*, 31(2):87–106.

Newman, M. (2010). *Networks: An Introduction*. Oxford University Press, Oxford.

Novta, N. and Pugacheva, E. (2021). Geopolitical risks and capital flows to emerging markets. *Journal of International Money and Finance*, 115:102391.

O’Malley, T., Bursztein, E., Long, H., Chollet, F., Jin, J., Invernizzi, L., et al. (2019). Kerastuner. <https://github.com/keras-team/keras-tuner>. Accessed: 2024-06-01.

Pastor, L. and Veronesi, P. (2021). Inequality aversion, populism, and the backlash against globalization. *The Journal of Finance*, 76(6):2857–2906.

Pesaran, M. H. and Shin, Y. (1998). Generalized impulse response analysis in linear multivariate models. *Economics Letters*, 58(1):17–29.

Reinhart, C. M., Rogoff, K. S., and Savastano, M. A. (2003). Debt intolerance. *Brookings Papers on Economic Activity*, 2003(1):1–74.

Rey, H. (2013). Dilemma not trilemma: The global financial cycle and monetary policy independence. *Proceedings of the Jackson Hole Economic Policy Symposium*, pages 285–333.

Ribeiro, M. T., Singh, S., and Guestrin, C. (2016). “why should i trust you?”: Explaining the predictions of any classifier. In *Proceedings of the 22nd ACM SIGKDD International Conference on Knowledge Discovery and Data Mining (KDD ’16)*, pages 1135–1144, New York, NY, USA. ACM.

Shapley, L. S. (1953). A value for n-person games. *Contributions to the Theory of Games*, 2:307–317.

Stock, J. H. and Watson, M. W. (2002). Forecasting using principal components from a large number of predictors. *Journal of the American Statistical Association*, 97(460):1167–1179.

Stock, J. H. and Watson, M. W. (2003). Forecasting output and inflation: The role of asset prices. *Journal of Economic Literature*, 41(3):788–829. Add full details as needed.

Swanson, E. T. (2021). Measuring the effects of federal reserve forward guidance and asset purchases on financial markets. *Journal of Monetary Economics*, 118:32–53.

Teräsvirta, T. (1994). Specification, estimation, and evaluation of smooth transition autoregressive models. *Journal of the American Statistical Association*, 89(425):208–218.

Tibshirani, R. (1996). Regression shrinkage and selection via the lasso. *Journal of the Royal Statistical Society: Series B (Methodological)*, 58(1):267–288.

Varian, H. R. (2014). Big data: New tricks for econometrics. *Journal of Economic Perspectives*, 28(2):3–28.

Zou, H. and Hastie, T. (2005). Regularization and variable selection via the elastic net. *Journal of the Royal Statistical Society: Series B (Statistical Methodology)*, 67(2):301–320.

A APPENDIX A: The data

This annex details country-specific data availability, as well as percentile distributions by country (Appendix A.1), as well as the procedures employed for the construction of the news-based indicators used in the empirical analysis (Appendix A.2).

A.1 Data availability by country

We include a summary describing the basis for the empirical analysis developed in the paper. Table XX presents country-specific data availability together with descriptive statistics summarizing the distribution of the main variables. For each country, the start and end dates of the available sample are reported. To characterize the distribution, we provide the 25th and 75th percentiles (p25 and p75), which capture the interquartile range where the central 50% of observations lie, for each of the described variables in the data section.

Figure 11: Country-specific sample periods and interquartile distributions of variables

Country	Sample		CDS		Global financial var.				Macroeconomic sentiment var.								Political and Geop. var.			
	Start	End	CDS		FED		VIX		ECO		INT		EPU		TPU		GPR		POL	
			p25	p75	p25	p75	p25	p75	p25	p75	p25	p75	p25	p75	p25	p75	p25	p75	p25	p75
Argentina	11/08/2020	13/06/2025	-0.78	0.77	-1.30	0.79	-0.72	0.60	-0.72	0.77	-0.39	0.68	-0.68	0.29	-0.77	0.66	-0.82	0.70	-0.76	0.52
Australia	01/01/2018	13/06/2025	-0.64	0.66	-1.03	0.99	-0.71	0.41	-0.34	0.61	-0.49	0.70	-0.65	0.30	-0.63	0.41	-0.69	0.58	-0.72	0.58
Austria	01/01/2018	13/06/2025	-0.95	0.64	-1.03	0.99	-0.71	0.41	-0.39	0.61	-0.39	0.66	-0.64	0.27	-0.56	0.21	-0.57	0.33	-0.69	0.61
Belgium	01/01/2018	13/06/2025	-0.82	0.63	-1.03	0.99	-0.71	0.41	-0.34	0.64	-0.36	0.67	-0.69	0.48	-0.71	0.53	-0.58	0.44	-0.67	0.45
Brazil	01/01/2018	13/06/2025	-0.73	0.66	-1.03	0.99	-0.71	0.41	-0.37	0.67	-0.38	0.67	-0.76	0.57	-0.76	0.52	-0.70	0.57	-0.72	0.47
Canada	21/02/2019	14/06/2025	-0.82	0.78	-1.19	0.96	-0.68	0.44	-0.41	0.68	-0.36	0.68	-0.54	0.16	-0.44	-0.05	-0.72	0.61	-0.75	0.57
Chile	01/01/2018	13/06/2025	-0.65	0.43	-1.03	0.99	-0.71	0.41	-0.62	0.72	-0.52	0.55	-0.73	0.54	-0.69	0.60	-0.67	0.54	-0.85	0.61
China	01/01/2018	13/06/2025	-0.79	0.57	-1.03	0.99	-0.71	0.41	-0.73	0.79	-0.50	0.76	-0.64	0.37	-0.58	0.45	-0.75	0.58	-0.55	0.52
Colombia	01/01/2018	13/06/2025	-0.91	0.67	-1.03	0.99	-0.71	0.41	-0.29	0.58	-0.21	0.50	-0.75	0.54	-0.67	0.52	-0.69	0.49	-0.74	0.66
CzechRep	01/01/2018	13/06/2025	-0.78	0.80	-1.03	0.99	-0.71	0.41	-0.45	0.54	-0.04	0.34	-0.68	0.45	-0.69	0.69	-0.70	0.44	-0.68	0.57
Denmark	01/01/2018	13/06/2025	-0.74	0.49	-1.03	0.99	-0.71	0.41	-0.50	0.71	-0.29	0.60	-0.72	0.46	-0.70	0.51	-0.64	0.45	-0.62	0.41
Egypt	01/01/2018	13/06/2025	-0.74	0.30	-1.03	0.99	-0.71	0.41	-0.44	0.56	-0.33	0.51	-0.68	0.54	-0.67	0.58	-0.75	0.49	-0.66	0.47
Finland	01/01/2018	13/06/2025	-0.79	0.80	-1.03	0.99	-0.71	0.41	-0.46	0.69	-0.57	0.73	-0.68	0.47	-0.70	0.49	-0.70	0.48	-0.58	0.51
France	01/01/2018	13/06/2025	-0.78	0.55	-1.03	0.99	-0.71	0.41	-0.29	0.60	-0.36	0.61	-0.49	0.10	-0.67	0.47	-0.60	0.44	-0.79	0.59
Germany	01/01/2018	13/06/2025	-0.69	0.34	-1.03	0.99	-0.71	0.41	-0.41	0.66	-0.38	0.66	-0.67	0.36	-0.72	0.58	-0.61	0.40	-0.69	0.59
Hungary	01/01/2018	13/06/2025	-0.75	0.52	-1.03	0.99	-0.71	0.41	-0.50	0.64	-0.15	0.56	-0.69	0.55	-0.71	0.48	-0.57	0.31	-0.60	0.49
India	01/01/2018	13/06/2025	-0.59	0.47	-1.03	0.99	-0.71	0.41	-0.46	0.63	-0.42	0.71	-0.67	0.38	-0.69	0.47	-0.66	0.46	-0.75	0.59
Indonesia	01/01/2018	13/06/2025	-0.72	0.42	-1.03	0.99	-0.71	0.41	-0.64	0.63	-0.28	0.62	-0.62	0.25	-0.61	0.38	-0.66	0.58	-0.67	0.60
Israel	01/01/2018	13/06/2025	-0.75	0.17	-1.03	0.99	-0.71	0.41	-0.49	0.74	-0.38	0.70	-0.69	0.51	-0.52	-0.06	-0.74	0.57	-0.86	0.59
Italy	01/01/2018	13/06/2025	-0.83	0.58	-1.03	0.99	-0.71	0.41	-0.43	0.74	-0.17	0.61	-0.79	0.58	-0.54	0.09	-0.62	0.44	-0.63	0.37
Japan	01/01/2018	13/06/2025	-0.71	0.47	-1.03	0.99	-0.71	0.41	-0.42	0.68	-0.40	0.68	-0.75	0.58	-0.75	0.45	-0.73	0.52	-0.70	0.38
Jordan	27/10/2023	13/06/2025	-0.63	0.55	-0.83	0.87	-0.76	0.41	-0.64	0.49	-0.36	0.64	-0.65	0.26	-0.73	0.65	-0.78	0.59	-0.63	0.63
Malaysia	01/01/2018	13/06/2025	-0.78	0.57	-1.03	0.99	-0.71	0.41	-0.66	0.63	-0.43	0.66	-0.66	0.30	-0.72	0.55	-0.84	0.69	-0.68	0.68
Mexico	01/01/2018	13/06/2025	-0.66	0.34	-1.03	0.99	-0.71	0.41	-0.35	0.64	-0.27	0.60	-0.72	0.66	-0.59	0.19	-0.69	0.58	-0.64	0.53
Morocco	01/01/2018	13/06/2025	-0.56	0.17	-1.03	0.99	-0.71	0.41	-0.56	0.52	-0.16	0.42	-0.74	0.61	-0.69	0.62	-0.68	0.52	-0.66	0.58
Netherlands	01/01/2018	13/06/2025	-0.79	0.35	-1.03	0.99	-0.71	0.41	-0.70	0.72	-0.32	0.64	-0.74	0.51	-0.74	0.52	-0.64	0.49	-0.67	0.43
Norway	01/01/2018	13/06/2025	-0.71	0.44	-1.03	0.99	-0.71	0.41	-0.45	0.73	-0.27	0.62	-0.70	0.38	-0.63	0.14	-0.65	0.57	-0.80	0.66
Peru	01/01/2018	13/06/2025	-0.53	0.37	-1.03	0.99	-0.71	0.41	-0.39	0.60	-0.31	0.62	-0.59	0.22	-0.64	0.45	-0.60	0.43	-0.64	0.36
Philippines	01/01/2018	13/06/2025	-0.78	0.69	-1.03	0.99	-0.71	0.41	-0.52	0.75	-0.20	0.54	-0.61	0.35	-0.71	0.51	-0.76	0.68	-0.69	0.45
Poland	01/01/2018	13/06/2025	-0.52	0.00	-1.03	0.99	-0.71	0.41	-0.45	0.69	-0.37	0.65	-0.74	0.51	-0.64	0.40	-0.71	0.50	-0.73	0.67
Qatar	01/01/2018	13/06/2025	-0.65	0.49	-1.03	0.99	-0.71	0.41	-0.65	0.49	-0.12	0.47	-0.64	0.25	-0.68	0.46	-0.75	0.36	-0.54	0.40
Russia	01/01/2018	06/04/2022	-0.21	-0.11	-1.08	1.02	-0.67	0.36	-0.15	0.61	0.01	0.48	-0.76	0.51	-0.67	0.45	-0.50	0.36	-0.62	0.30
SaudiA.	01/01/2018	13/06/2025	-0.65	0.46	-1.03	0.99	-0.71	0.41	-0.42	0.56	-0.14	0.55	-0.76	0.53	-0.73	0.55	-0.73	0.57	-0.55	0.44
Spain	01/01/2018	13/06/2025	-0.76	0.38	-1.03	0.99	-0.71	0.41	-0.35	0.65	-0.27	0.58	-0.65	0.39	-0.52	0.27	-0.63	0.41	-0.67	0.51
Sweden	01/01/2018	13/06/2025	-0.71	0.83	-1.03	0.99	-0.71	0.41	-0.53	0.69	-0.41	0.68	-0.71	0.45	-0.45	0.11	-0.64	0.52	-0.76	0.60
Thailand	01/01/2018	13/06/2025	-0.55	0.31	-1.03	0.99	-0.71	0.41	-0.44	0.72	-0.25	0.50	-0.60	0.36	-0.42	0.19	-0.68	0.43	-0.28	0.59
Turkey	01/01/2018	13/06/2025	-0.77	0.73	-1.03	0.99	-0.71	0.41	-0.46	0.64	-0.20	0.53	-0.66	0.47	-0.68	0.50	-0.74	0.59	-0.47	0.56
UK	01/01/2018	13/06/2025	-0.71	0.72	-1.03	0.99	-0.71	0.41	-0.39	0.69	-0.43	0.69	-0.65	0.44	-0.55	0.34	-0.62	0.39	-0.66	0.41
USA	01/01/2018	13/06/2025	-0.79	0.76	-1.03	0.99	-0.71	0.41	-0.17	0.58	-0.45	0.70	-0.62	0.28	-0.69	0.41	-0.63	0.50	-0.72	0.51
Ukraine	17/01/2020	06/04/2022	-0.33	-0.14	-0.54	0.09	-0.73	0.28	-0.41	0.70	0.15	0.47	-0.81	0.59	-0.72	0.47	-0.69	0.29	-0.67	0.67
Uruguay	01/01/2018	13/06/2025	-0.75	0.45	-1.03	0.99	-0.71	0.41	-0.49	0.65	-0.48	0.69	-0.71	0.51	-0.62	0.59	-0.72	0.54	-0.79	0.65
Vietnam	01/01/2018	13/06/2025	-0.69	0.40	-1.03	0.99	-0.71	0.41	-0.70	0.64	-0.60	0.66	-0.68	0.35	-0.65	0.26	-0.78	0.75	-0.23	0.56

A.2 Media sentiment indicators development process

All indices are developed by BBVA Research using the Global Database of Events, Language, and Tone (GDELT) as described previously in the data section. The indices are daily and collected at the country level. To ensure homogeneity, each index is normalized (minus average and divided by standard deviation) and smoothed using a 28-day moving average. This transformation reduces daily noise and allows for a clearer identification of signals. No outlier treatment is performed, since the objective is to capture events that stand out from the normal behavior of the indicators.

The detailed set of keywords included in each case to build the indicators are the following:

- Economic Policy Uncertainty (EPU) Index

The Economic Policy Uncertainty (EPU) Index is originally constructed by BBVA Research based on the relative coverage associated with GDELT searches using country-specific keywords. The specific choice of keywords for each country aims to replicate the methodology presented by Baker, Bloom and Davis (2016) in "Measuring Economic Policy Uncertainty".

- United States: "United States (uncertainty OR uncertain) (economic OR economy) (congress OR legislation OR white house OR regulation OR federal reserve OR deficit)"
- China: "China (uncertain OR uncertainty) (economy OR economic OR business) (fiscal OR monetary OR Commission OR bank OR legislation OR tax OR bonds OR debt OR tariff OR deficit)"
- Canada: "Canada (uncertain OR uncertainty)(economic OR economy)(policy OR tax OR spending OR regulation OR central bank OR budget OR deficit)"
- Mexico: "Mexico (economic OR economy) (uncertain OR uncertainty) (regulation OR deficit OR budget OR Bank OR BdeM OR Banxico OR congress OR senate OR deputies OR legislation OR taxes OR Federal Reserve)"
- Spain: "Spain (uncertainty OR uncertain OR instability OR risk) (economic OR economy) (parliament OR government OR Hacienda OR deficit OR budget OR expenditure OR debt OR taxes OR law OR reform OR regulation OR Bank)"
- Australia: "Australia (uncertain OR uncertainty) (economic OR economy) (regulation OR Reserve Bank of Australia OR RBA OR deficit OR tax OR taxation OR taxes OR parliament OR senate OR cash rate OR legislation OR tariff OR war)"
- Brazil: "Brazil (uncertain OR uncertainty) (economic OR economy) (regulation OR deficit OR budget OR tax OR central bank OR Alvorada OR Planalto OR congress OR senate OR deputies OR legislation OR law OR tariff)"
- Chile: "Chile (uncertain OR uncertainty) (economic OR economy) (politics OR tax OR regulation OR reform OR congress OR senate OR spending OR debt OR budget OR Central Bank OR Ministry of Finance)"
- Colombia: "Colombia (economy OR economic) (uncertainty OR uncertain) (politics OR politician OR government OR tax OR reform OR deficit OR debt OR spending OR congress OR crisis OR Bank OR Ministry OR corruption OR peace OR conflict OR subsidy)"
- France: "France (uncertain OR uncertainty) (economic OR economy) (congress OR legislation OR regulation OR central bank OR ECB OR deficit)"
- Germany: "Germany (uncertain OR uncertainty) (economic OR economy) (congress OR legislation OR regulation OR central bank OR ECB OR deficit)"
- India: "India (uncertain OR uncertainty OR uncertainties) (economic OR economy) (regulation OR central bank OR monetary policy OR policymakers OR deficit OR legislation OR fiscal policy)"
- Pakistan: "Pakistan (uncertainty OR uncertain OR unpredictable OR unclear OR unstable) (economics OR economy) (regulation OR policy OR bank OR SBP OR FBR OR tax OR parliament OR deficit OR government OR reserves OR taxes OR legislation)"
- Russia: "Russia (uncertain OR uncertainty) (economic OR economy) (policy OR tax OR spending OR regulation OR central bank OR law OR Duma OR budget)"
- Turkey: "Turkey (uncertain OR uncertainty) (economic OR economy)"
- United Kingdom: "(United Kingdom OR UK) (uncertain OR uncertainty) (economic OR economy) (policy OR tax OR spending OR regulation OR Bank of England OR budget OR deficit)"
- All other countries: "COUNTRY_NAME (uncertain OR uncertainty) (economic OR economy) (policy OR tax OR spending OR regulation OR central bank OR budget OR deficit)"

The constructed index corresponds to the relative coverage (number of news related to EPU / total number of published news). The indices are smoothed with a 28-day moving average and normalized.

- Political Tensions Index

The Political Tensions Index is originally constructed by BBVA Research based on the tone and coverage associated with GDELT searches of keywords for: political instability, political uncertainty, political crisis, political polarization, political extremism, political turmoil, political conflict. Additionally, the index uses the GDELT taxonomy USPEC_POLITICS_GENERAL1, which includes news related to: Elections and campaigns, Political parties and politicians, Government institutions and branches, Executive orders and presidential actions, Congressional activities and legislation, Supreme Court decisions and judicial appointments, Political scandals and corruption, Civil rights and social justice issues, Foreign policy and international relations, National security and defense policy, Immigration policy and border security, Healthcare policy and reform, Environmental policy and regulation, Tax policy and reform, Gun control and firearms policy, Education policy and reform, Infrastructure policy and investment, Social welfare policy and programs, Civil liberties and privacy concerns, Political polarization and partisanship.

The keywords contained in the query use “OR” statements so that the mention of any of them returns news articles containing any one of them, provided the articles are classified within the GDELT taxonomy theme USPEC_POLITICS_GENERAL1.

The index is a weighted product of tone (sentiment) and relative coverage and it is multiplied by -1 for interpretability.

- Geopolitical Risk (GPR) Index

The Geopolitical Risk Index is originally constructed by BBVA Research based on the tone and coverage associated with GDELT searches, following the methodology of Caldara and Iacoviello (2022).

The data should contain at least one theme included in the GDELT taxonomy of each group:

- Group 1: war, conflict, hostvisit, revolutionary violence, appraiser, rebellion, violent unrest, peacekeeping, mutual recognition agreements, ceasefire, treaties, parliament and legislatures, military, troop, nuclear-power, hydropower, terror, rebels guerrillas and insurgents, kidnap, alliance, group popular resistance committee, insurgency, group social resistance, military cooperation, navy, aerial photographer, rebels.
- Group 2: act harmthreaten, advertiser, risk, concern worldwide, speciesendangered, crisis, trouble, dispute boards, dismissal procedures, boycott, disruption, slfid military buildup, sanctions, blockade, financial vulnerability and risks, soc quarantine, unrest ultimatum, makestatement, outbreak, announcer, armourer, persecution, crash, raid, armedconflict, act forceposttrue, bombthreat, kill, strike.

The index is a weighted product of tone (sentiment) and relative coverage and it is multiplied by -1 for interpretability.

- Trade Policy Uncertainty (TPU) Index

The Trade Policy Uncertainty (TPU) Index is originally constructed by BBVA Research based on the relative coverage associated with GDELT searches using the following set of keywords:

(tariff OR tariffs OR import OR imports OR export OR exports OR trade OR dumping OR antidumping OR GATT OR WTO) (duty OR duties OR barrier OR barriers OR ban OR bans OR tax OR taxes OR subsidy OR subsidies)

This keyword set replicates the methodology proposed by Caldara, Iacoviello, Molligo, Prestipino, and Raffo (2020) in “The Economic Effects of Trade Policy Uncertainty”.

The constructed index corresponds to the relative coverage (number of TPU-related news / total number of published news). The indices are smoothed with a 28-day moving average and normalized.

B Appendix B. Machine-Learning Forecast Evaluation

This appendix provides technical details on the evaluation of the machine-learning forecasts used in the main text. We set out the notation for the unbalanced panel, define the loss functions, and formalize how we compute aggregate accuracy measures and the incremental predictive value of news-based indicators.

B.1 Panel Notation and Forecast Errors

Let $i = 1, \dots, N$ index countries and t index trading days. For each country i and date t , let $y_{i,t}$ denote the standardized CDS spread, and $X_{i,t}$ the corresponding vector of predictors (global financial variables and news-based indicators). For a given model class m and information set k (Markets-only or Markets+News), we write the one-step-ahead forecast of $y_{i,t+1}$ as

$$\hat{y}_{i,t+1}^{(m,k)} = \hat{f}^{(m,k)}(X_{i,t}),$$

where $\hat{f}^{(m,k)}$ is estimated only using information available up to time t in a recursive (pseudo-real time) scheme.

The corresponding forecast error is

$$e_{i,t+1}^{(m,k)} = y_{i,t+1} - \hat{y}_{i,t+1}^{(m,k)}, \quad (i, t) \in \mathcal{S}_{\text{roll}}, \quad (6)$$

where $\mathcal{S}_{\text{roll}}$ denotes the set of out-of-sample forecast origins generated by the recursive rolling procedure. Because we work with an unbalanced panel and with 28-day moving averages, the recursive scheme is implemented with a 28-day buffer around each train–test split to avoid overlap between training and test windows.

B.2 Loss Functions: MAE and RMSE

We summarize forecast accuracy using the Mean Absolute Error (MAE) and the Root Mean Squared Error (RMSE) computed over the out-of-sample panel.

Pooled (micro) metrics. Pooling all country–day observations in $\mathcal{S}_{\text{roll}}$, the pooled MAE and RMSE for model m under information set k are defined as

$$\text{MAE}_{\text{pool}}^{(m,k)} = \frac{1}{|\mathcal{S}_{\text{roll}}|} \sum_{(i,t) \in \mathcal{S}_{\text{roll}}} |e_{i,t+1}^{(m,k)}|, \quad (7)$$

$$\text{RMSE}_{\text{pool}}^{(m,k)} = \left[\frac{1}{|\mathcal{S}_{\text{roll}}|} \sum_{(i,t) \in \mathcal{S}_{\text{roll}}} (e_{i,t+1}^{(m,k)})^2 \right]^{1/2}. \quad (8)$$

The square root in (8) ensures that RMSE is expressed in the same units as the dependent variable $y_{i,t}$.

Country-level metrics. To characterize heterogeneity across countries, we also compute MAE and RMSE at the country level. For each country i , let

$$\mathcal{S}_{\text{roll}}(i) = \{t : (i, t) \in \mathcal{S}_{\text{roll}}\}$$

denote the set of out-of-sample forecast dates available for i . We define

$$\text{MAE}_i^{(m,k)} = \frac{1}{|\mathcal{S}_{\text{roll}}(i)|} \sum_{t \in \mathcal{S}_{\text{roll}}(i)} |e_{i,t+1}^{(m,k)}|, \quad (9)$$

$$\text{RMSE}_i^{(m,k)} = \left[\frac{1}{|\mathcal{S}_{\text{roll}}(i)|} \sum_{t \in \mathcal{S}_{\text{roll}}(i)} (e_{i,t+1}^{(m,k)})^2 \right]^{1/2}. \quad (10)$$

We then report *average* country-level metrics across the cross-section:

$$\overline{\text{MAE}}_{\text{ctry}}^{(m,k)} = \frac{1}{N} \sum_{i=1}^N \text{MAE}_i^{(m,k)}, \quad (11)$$

$$\overline{\text{RMSE}}_{\text{ctry}}^{(m,k)} = \frac{1}{N} \sum_{i=1}^N \text{RMSE}_i^{(m,k)}. \quad (12)$$

In practice, when countries differ in the length of their available history, we also report averages over balanced subsamples to check robustness.

Regional metrics. For some results we aggregate performance by region $r \in \mathcal{R}$ (Advanced Economies, EM Asia, EM Latin America, EM Europe, EM MENA). Let \mathcal{I}_r be the set of countries in region r . Regional averages are computed as

$$\overline{\text{MAE}}_r^{(m,k)} = \frac{1}{|\mathcal{I}_r|} \sum_{i \in \mathcal{I}_r} \text{MAE}_i^{(m,k)}, \quad (13)$$

$$\overline{\text{RMSE}}_r^{(m,k)} = \frac{1}{|\mathcal{I}_r|} \sum_{i \in \mathcal{I}_r} \text{RMSE}_i^{(m,k)}. \quad (14)$$

B.3 Incremental Value of News

The main text compares a Markets-only information set and an augmented Markets+News specification. For each model class m and each evaluation unit (pooled, country, or region), we define the incremental contribution of news as the change in MAE and RMSE when moving from Markets-only to Markets+News.

Levels. Let $k \in \{\text{Mkt}, \text{Mkt+News}\}$ denote the information set. The level improvement in MAE for model m is

$$\Delta\text{MAE}^{(m)} = \text{MAE}^{(m, \text{Mkt})} - \text{MAE}^{(m, \text{Mkt+News})}, \quad (15)$$

with an analogous definition for RMSE:

$$\Delta\text{RMSE}^{(m)} = \text{RMSE}^{(m, \text{Mkt})} - \text{RMSE}^{(m, \text{Mkt+News})}. \quad (16)$$

Positive values of $\Delta\text{MAE}^{(m)}$ or $\Delta\text{RMSE}^{(m)}$ indicate that news-based indicators improve forecast accuracy relative to the FED+VIX benchmark.

Percent improvements. For ease of interpretation, we often report percentage gains:

$$\% \Delta\text{MAE}^{(m)} = 100 \times \frac{\text{MAE}^{(m, \text{Mkt})} - \text{MAE}^{(m, \text{Mkt+News})}}{\text{MAE}^{(m, \text{Mkt})}}, \quad (17)$$

$$\% \Delta\text{RMSE}^{(m)} = 100 \times \frac{\text{RMSE}^{(m, \text{Mkt})} - \text{RMSE}^{(m, \text{Mkt+News})}}{\text{RMSE}^{(m, \text{Mkt})}}. \quad (18)$$

Analogous formulas apply when the underlying MAE and RMSE are computed at the country or regional level as in (11)–(12). The tables in the main text and online appendix report both level and percentage improvements for each model class and region.

C APPENDIX C: Machine Learning Models

This appendix documents the models used in the forecasting evaluation. For each class, we summarize the functional form and the selection strategy for hyperparameters. Models are estimated on an unbalanced panel of sovereign CDS spreads, $y_{i,t+1}$, using country-level predictors $\mathbf{X}_{i,t}$. Predictors include global financial variables (U.S. 2-year yield and VIX), the Geopolitical Risk Index, local macroeconomic sentiment variables (economic and interest rate sentiment), local economic and trade uncertainty indices, and the Political Tensions Index.

C.1 Hyperparameter Search

Hyperparameter optimization was conducted using a Bayesian optimization approach, in particular the one implemented by the Optuna framework. However, the temporal nature of the dataset required a deviation from standard evaluation protocols. Standard k -fold cross-validation was unsuitable because random partitioning disrupts the chronological order of observations. This introduces look-ahead bias, as it allows the model to train on future information to predict past events.

Designing the validation split required balancing training set size with temporal generalization. A simple chronological segmentation—splitting the timeline into equal segments—was rejected because the earliest folds would yield training sets too small for effectively training complex models. This was particularly true for countries with limited historical data. Conversely, selecting validation folds strictly from the very end of the dataset to maximize sample size would restrict evaluation to a narrow, recent timeframe, failing to capture diverse temporal regimes or seasonal shifts.

To address these constraints, we implemented a custom expanding window cross-validation scheme. We selected five validation dates starting from the end of the available training data and stepping backward by fixed intervals of 60 days. This 60-day step ensures that validation folds are sufficiently spaced to assess performance across different market conditions. Furthermore, this expanding window approach ensures that even the earliest split utilizes a substantial portion of the historical data, guaranteeing sufficient sample sizes for stable model convergence.

Finally, a strict separation between training and validation sets was enforced to prevent data leakage. Since the feature engineering pipeline incorporates moving averages calculated over a 28-day window, immediate adjacency between training and validation data would result in feature contamination. To prevent this, a 28-day buffer period was applied; for any given validation date t , the training set excluded all observations from the preceding 28 days (ending at $t - 28$), strictly isolating the validation target from the training process.

C.2 Linear and Regularized Models

These models assume a linear relationship between predictors $\mathbf{X}_{i,t}$ and one-step-ahead sovereign risk $y_{i,t+1}$. Given the dimensionality of predictors and potential collinearity, we consider both OLS and regularized variants (Hastie et al., 2009). The panel has relatively few cross-sectional units (N) but a long time dimension (T), so nonlinearities are more likely to arise from temporal rather than cross-sectional complexity.

Fixed Effects OLS.

As a baseline, we estimate pooled panel regressions with country fixed effects and common slope coefficients across countries and time:

$$y_{i,t+1} = \alpha_i + \boldsymbol{\theta}^\top \mathbf{X}_{i,t} + \varepsilon_{i,t+1}, \quad (19)$$

where α_i denotes a country-specific intercept and $\boldsymbol{\theta}$ the common coefficient vector.

Lasso.

The Lasso estimator (Tibshirani, 1996) in the fixed effects setting solves

$$\hat{\boldsymbol{\theta}}^{\text{Lasso}} = \arg \min_{\boldsymbol{\theta}} \left\{ \sum_{i,t} (y_{i,t+1} - \alpha_i - \boldsymbol{\theta}^\top \mathbf{X}_{i,t})^2 + \lambda \|\boldsymbol{\theta}\|_1 \right\}. \quad (20)$$

The L1 penalty shrinks coefficients and performs variable selection. In our implementation, the result of the hyperparameter search was $\lambda = 0.027$ in the news extended case and $\lambda = 0.018$ in the market variables only case.

Ridge.

Ridge regression (Hoerl and Kennard, 1970) with fixed effects penalizes the squared Euclidean norm of the slope vector:

$$\hat{\boldsymbol{\theta}}^{\text{Ridge}} = \arg \min_{\boldsymbol{\theta}} \left\{ \sum_{i,t} (y_{i,t+1} - \alpha_i - \boldsymbol{\theta}^\top \mathbf{X}_{i,t})^2 + \lambda \|\boldsymbol{\theta}\|_2^2 \right\}. \quad (21)$$

The estimated penalty parameter was $\lambda = 1000$ in the news extended case and $\lambda = 0.010$ in the market variables only case.

Elastic Net.

The Elastic Net (Zou and Hastie, 2005) combines the Lasso and Ridge penalties in the fixed effects model:

$$\hat{\boldsymbol{\theta}}^{\text{EN}} = \arg \min_{\boldsymbol{\theta}} \left\{ \sum_{i,t} (y_{i,t+1} - \alpha_i - \boldsymbol{\theta}^\top \mathbf{X}_{i,t})^2 + \lambda [\rho \|\boldsymbol{\theta}\|_1 + (1 - \rho) \|\boldsymbol{\theta}\|_2^2] \right\}. \quad (22)$$

Here $\rho \in [0, 1]$ controls the L1/L2 trade-off. In our setting, $\lambda = 0.034$ and $\rho = 0.82$ in the news extended case, and $\lambda = 0.016$ and $\rho = 0.94$ in the market variables only case.

Quantile Regression.

To capture distributional heterogeneity in CDS spreads, we estimate fixed effects quantile regressions (Koenker and Bassett, 1978). For quantile level τ :

$$Q_\tau(y_{i,t+1} | \mathbf{X}_{i,t}) = \alpha_{i,\tau} + \boldsymbol{\theta}_\tau^\top \mathbf{X}_{i,t}, \quad (23)$$

with estimator

$$(\{\hat{\alpha}_{i,\tau}\}, \hat{\boldsymbol{\theta}}_\tau) = \arg \min_{(\{\alpha_i\}, \boldsymbol{\theta})} \sum_{i,t} \rho_\tau \left(y_{i,t+1} - \alpha_i - \boldsymbol{\theta}^\top \mathbf{X}_{i,t} + \lambda \sum_j |\theta_j| \right), \quad (24)$$

where we have included a regularisation term, and $\rho_\tau(u) = u(\tau - \mathbf{1}\{u < 0\})$. We fix $\tau = 0.5$, and $\lambda = 0.019$ in the news extended case, and $\lambda =$ in the market variables only case.

C.3 Principal Components Regression and Factor Models

These methods reduce the dimensionality of predictors by extracting latent components that capture most of the relevant information, mitigating multicollinearity and improving parsimony (Stock and Watson, 2003). Estimation is again based on minimizing mean squared error, but with predictors replaced by latent components.

Principal Component Regression (PCR).

PCR applies PCA to the set of regressors $\mathbf{X}_{i,t}$, retaining K components (47 in the news extended case and 43 in the market variables only case). Country fixed effects are then added, and the response is regressed on the resulting scores (Jolliffe, 2002):

$$y_{i,t+1} = \alpha_i + \phi^\top \mathbf{t}_{i,t} + \varepsilon_{i,t+1}, \quad (25)$$

where $\mathbf{t}_{i,t}$ is the K -dimensional vector of principal component scores. The estimator solves

$$\hat{\phi} = \arg \min_{\phi} \sum_{i,t} (y_{i,t+1} - \alpha_i - \phi^\top \mathbf{t}_{i,t})^2.$$

Factor Analysis with Ridge (FAR).

We first extract latent factors (13 in the news extended case and 20 in the market variables only case) via factor analysis,

$$\mathbf{X}_{i,t} = \Lambda \mathbf{f}_{i,t} + \varepsilon_{i,t}, \quad \varepsilon_{i,t} \sim \mathcal{N}(0, \Psi).$$

Factor scores $\hat{f}_{i,t}$ are then used in a Ridge regression with country fixed effects:

$$\hat{\beta} = \arg \min_{\beta} \sum_{i,t} (y_{i,t+1} - \alpha_i - \beta^\top \hat{f}_{i,t})^2 + \lambda \|\beta\|_2^2.$$

with $\lambda = 25$ in the news extended case and $\lambda = 3.5$ in the market variables only case.

C.4 Tree-Based Ensemble Methods

Tree-based ensembles approximate complex nonlinear functions by combining the predictions of multiple decision trees. Each individual tree partitions the predictor space into regions and assigns a constant prediction within each region. Different ensemble constructions (bagging, random feature selection, boosting, or randomization of split thresholds) yield distinct bias–variance trade-offs (Hastie et al., 2009). All models are trained to minimize mean squared error. With the exception of the gradient boosting case, where it was optimized during the hyperparameter search, the number of estimators was set to 1000.

Gradient Boosting (GB).

Gradient Boosting builds an additive predictor

$$F_b(\mathbf{X}_{i,t}) = F_{b-1}(\mathbf{X}_{i,t}) + \nu f_b(\mathbf{X}_{i,t}), \quad (26)$$

where f_b is the regression tree fitted at stage b , ν the learning rate, and B the total number of boosting rounds. The final estimator is obtained by minimizing squared-error loss:

$$\hat{F} = \arg \min_{F \in \mathcal{F}_{\text{Boost}}} \sum_{i,t} (y_{i,t+1} - F(\mathbf{X}_{i,t}))^2. \quad (27)$$

The hyperparameters used after optimising them can be found in Table 2.

Bagging.

Bagging averages the predictions of B bootstrap-sampled trees:

$$\hat{y}_{i,t+1}^{(\text{Bag})} = \frac{1}{B} \sum_{b=1}^B \hat{f}_b(\mathbf{X}_{i,t}), \quad (28)$$

where each base tree \hat{f}_b is trained on a bootstrap subsample \mathcal{D}_b . Each tree is estimated by

$$\hat{f}_b = \arg \min_{f \in \mathcal{F}_{\text{Tree}}} \sum_{(i,t) \in \mathcal{D}_b} (y_{i,t+1} - f(\mathbf{X}_{i,t}))^2. \quad (29)$$

The hyperparameters used can be found in Table 3.

	News extended case	Market variables only case
Number of trees	535	145
Learning rate	0.012	0.034
Max Depth	8	5
Subsample Ratio	0.97	0.68
Feature Subset Size	0.62	0.69
Minimum Child Weight	3	2

Table 2: Gradient Boosting hyperparameters (used in the XGBoost implementation).

	News extended case	Market variables only case
Max Depth	40	6
Min Samples Split	5	14
Min Samples Leaf	8	3
Feature Subset Size	0.67	0.93

Table 3: Bagging hyperparameters.

Random Forest (RF).

Random Forests extend bagging by randomly selecting m_{try} predictors at each split. The ensemble predictor is

$$\hat{y}_{i,t+1}^{(\text{RF})} = \frac{1}{B} \sum_{b=1}^B \hat{f}_b(\mathbf{X}_{i,t}), \quad (30)$$

where each tree \hat{f}_b is trained on a bootstrap sample with restricted feature sets. Formally,

$$\hat{f}_b = \arg \min_{f \in \mathcal{F}_{\text{free}}^{m_{\text{try}}}} \sum_{(i,t) \in \mathcal{D}_b} (y_{i,t+1} - f(\mathbf{X}_{i,t}))^2. \quad (31)$$

The chosen hyperparameters can be seen in Table 4.

	News extended case	Market variables only case
Max Depth	60	115
Min Samples Split	5	4
Min Samples Leaf	4	20
Feature Subset Size	0.10	0.12

Table 4: Random Forest hyperparameters (used in the Scikit-learn Random Forest implementation).

Extremely Randomized Trees (ET).

ET increase randomization by drawing split thresholds at random. The ensemble predictor is

$$\hat{y}_{i,t+1}^{(\text{ET})} = \frac{1}{B} \sum_{b=1}^B \hat{f}_b(\mathbf{X}_{i,t}), \quad (32)$$

with each tree \hat{f}_b estimated by

$$\hat{f}_b = \arg \min_{f \in \mathcal{F}_{\text{free}}^{\text{Rand}}} \sum_{(i,t) \in \mathcal{D}_b} (y_{i,t+1} - f(\mathbf{X}_{i,t}))^2. \quad (33)$$

The values obtained in the hyperparameter search can be seen in Table 5.

Multilayer Random Forest (2S).

To capture heterogeneity across groups, we implement a hierarchical extension of Random Forests. In Stage 1, a forest \hat{f}_{AE} is trained on Advanced Economies (AE). In Stage 2, separate forests $\{\hat{f}_r : r \in \mathcal{R}\}$ are trained on Emerging Market

	News extended case	Market variables only case
Max Depth	139	128
Min Samples Split	3	6
Min Samples Leaf	1	10
Feature Subset Size	0.22	0.38

Table 5: Extremely Randomized Trees hyperparameters (used in the Scikit-learn implementation).

(EM) regions. Prediction is piecewise:

$$\hat{y}_{i,t+1}^{(\text{MLRF2})} = \begin{cases} \hat{f}_{\text{AE}}(\mathbf{X}_{i,t}) & \text{if } i \in \text{AE}, \\ \hat{f}_{\text{Region}(i)}(\mathbf{X}_{i,t}) & \text{if } i \in \text{EM}. \end{cases} \quad (34)$$

Each forest minimizes squared-error loss on its subsample:

$$\hat{f}_g = \arg \min_{f \in \mathcal{F}_{\text{RF}}} \frac{1}{n_g} \sum_{(i,t) \in \mathcal{D}_g} (y_{i,t+1} - f(\mathbf{X}_{i,t}))^2, \quad (35)$$

where $g \in \{\text{AE}\} \cup \mathcal{R}$. Equivalently, the composite loss minimized by the hierarchy is

$$\mathcal{L}_{\text{MLRF}}(\hat{f}_{\text{AE}}, \{\hat{f}_r\}) = \frac{1}{n_{\text{AE}}} \sum_{(i,t) \in \mathcal{D}_{\text{AE}}} (y_{i,t+1} - \hat{f}_{\text{AE}}(\mathbf{X}_{i,t}))^2 + \sum_{r \in \mathcal{R}} \frac{1}{n_r} \sum_{(i,t) \in \mathcal{D}_r} (y_{i,t+1} - \hat{f}_r(\mathbf{X}_{i,t}))^2. \quad (36)$$

The hyperparameters for these random forests can be seen in Table 6.

	News extended case	Market variables only case
Max Depth Stage 1	28	16
Subsample Ratio Stage 1	0.69	0.89
Feature Subset Size Stage 1	0.59	0.72
Minimum Child Weight Stage 1	17	20
Max Depth Stage 2	35	29
Subsample Ratio Stage 2	0.78	0.77
Feature Subset Size Stage 2	0.30	0.35
Minimum Child Weight Stage 2	14	50

Table 6: Multilayer Random Forest (2S) hyperparameters (used in the XGBoost Random Forest implementation).

Multilayer Random Forest (1S).

This one-stage alternative simplifies the hierarchical structure of the MLRF by treating all groups symmetrically. Instead of separating Advanced Economies from Emerging Markets in a stepwise fashion, we train an independent random forest \hat{f}_r for every region r (including AE and each EM sub-region) simultaneously. The prediction implies simply selecting the model corresponding to country i 's region:

$$\hat{y}_{i,t+1}^{(\text{MLRF1})} = \hat{f}_r(\mathbf{X}_{i,t}), \quad \text{for } i \in r. \quad (37)$$

This approach maintains the ability to capture cross-sectional heterogeneity but assumes that no shared global structure is required between AE and EM groups. As before, the advanced and emerging regions will have different hyperparameters, which can be seen in Table 7.

C.5 Convolutional Neural Networks (CNNs)

Neural networks approximate nonlinear mappings by composing linear transformations with nonlinear activations. Convolutional Neural Networks (CNNs) exploit local structure in predictors using convolutional filters, pooling layers, and dense layers. For input $\mathbf{X}_{i,t} \in \mathbb{R}^p$, the prediction function is

$$\hat{y}_{i,t+1} = g_{\theta}(\mathbf{X}_{i,t}),$$

with parameters θ estimated by minimizing mean squared error:

$$\hat{\theta} = \arg \min_{\theta} \sum_{i,t} (y_{i,t+1} - g_{\theta}(\mathbf{X}_{i,t}))^2. \quad (38)$$

	News extended case	Market variables case
Max Depth AE	27	15
Subsample Ratio AE	0.87	0.83
Feature Subset Size AE	0.73	0.67
Minimum Child Weight AE	10	23
Max Depth EM	41	24
Subsample Ratio EM	0.67	0.60
Feature Subset Size EM	0.35	0.36
Minimum Child Weight EM	14	40

Table 7: Multilayer Random Forest (1S) hyperparameters (used in the XGBoost Random Forest implementation).

Shallow CNN.

The architecture consists of a single convolutional layer configured with 64 filters and a kernel size of 5, using ReLU activation. This is followed by max pooling, flattening, and a dense hidden layer with 64 units in the news extended case, and 32 units in the market variables case. In the former, the learning rate was 0.0010 and the batch size 512, while in the latter the learning rate was 0.0055 and the batch size 256. All these values were obtained in the hyperparameter search. Overall, this setup is designed to capture simple localized interactions between predictors.

Deep CNN.

The architecture consists of a variable number of convolutional blocks. Each block comprises two 1D convolutional layers with causal padding and ReLU activations, followed by a max pooling layer (pool size 2). To capture increasingly complex patterns, the number of filters doubles with each subsequent block. Instead of flattening, global average pooling is applied after the final block, followed by a dense hidden layer and a single output unit. Hyperparameters such as the number of blocks, kernel size, and dense units are tuned using the Optuna framework (the exact values can be seen in Table 8), and the model is compiled with the Adam optimizer and MSE loss.

	News extended case	Market variables case
Number of convolutional blocks	2	2
Initial filter number	32	32
Kernel size	7	7
Number of dense units	128	64
Learning rate	0.0010	0.0018
Batch size	512	512

Table 8: Deep CNN hyperparameters.

Appendix C. Spillover and Network Interconnectedness Methodology

This appendix provides a complete technical description of the procedure used to construct (i) the Diebold–Yilmaz (DY) dynamic spillover index and (ii) the weighted network-density measure based on Spearman correlations. Both indices are computed directly from daily, country-level SHAP-implied risk attributions generated by the preferred machine-learning model. The procedures described below correspond exactly to the algorithms implemented in the empirical code.

C.1. Panel Construction and Pre-Processing

Let $s_{i,t}^{(f)}$ denote the SHAP-implied contribution of feature f to the CDS spread of country i on date t . The original SHAP panel is unbalanced and may contain missing days or countries with short histories. For each feature f , we construct a cleaned panel as follows:

1. **Weekly evaluation grid.** We define a sequence of center dates $\{t_0^{(m)}\}_{m=1}^M$ at 7-day intervals, beginning in January 2021.

2. **Coverage-based selection.** For each $t_0^{(m)}$, and feature f , we compute the *effective dimension* $k_{\text{eff}}(t_0)$, defined as the number of countries i such that $s_{i,t}^{(f)}$ is observed in at least 70% of days within a ± 180 -day probe window.

3. **Adaptive window length.** The window half-width $h(t_0)$ is set using the rule-of-thumb

$$T = 6k_{\text{eff}}p,$$

where $p = 3$ is the target lag length.¹⁹ The half-width is truncated:

$$h(t_0) \in [60, 180] \text{ days.}$$

4. **Window extraction.** For each t_0 , we take the sample $\mathcal{W}(t_0) = [t_0 - h(t_0), t_0 + h(t_0)]$.

5. **Data cleaning.** Within each window:

- (a) Linear interpolation is applied to fill short gaps.
- (b) Countries with low coverage (<70%) are dropped.
- (c) Countries with near-constant values (standard deviation $< 10^{-10}$) are dropped.
- (d) Remaining series are standardized:

$$\tilde{s}_{i,t}^{(f)} = \frac{s_{i,t}^{(f)} - \bar{s}_i^{(f)}}{\sigma_i^{(f)}}.$$

6. **Top- N selection.** If more than 10 countries remain, we retain up to

$$N_{\max} = 10,$$

choosing the countries with the highest coverage and cross-sectional variance.²⁰

C.2. VAR Estimation and Lag Selection

Let X_t denote the $k \times 1$ vector stacking the standardized SHAP series for the selected countries, evaluated on the rolling window $\mathcal{W}(t_0)$. A VAR(p) is estimated:

$$X_t = A_1 X_{t-1} + A_2 X_{t-2} + \cdots + A_p X_{t-p} + u_t,$$

where $u_t \sim (0, \Sigma_u)$.

Lags are selected according to the Akaike Information Criterion (AIC). At each window, the lag order p is selected via:

$$p^* = \arg \min_{p \in \{1, 2, 3, 4\}} \text{AIC}(p),$$

with a maximum of four lags allowed. The VAR lag order is not fixed *ex ante*: in each rolling window, the optimal lag length p^* is selected by the AIC from $p \in \{1, 2, 3, 4\}$, implying that the effective model order varies across features and dates depending on data coverage, window width, and the time-series structure of the Shapley value attributions.

Ridge stabilization. To ensure invertibility when computing generalized variance decompositions, the covariance matrix is regularized as:

$$\Sigma_u^\lambda = \Sigma_u + \lambda I, \quad \lambda = 10^{-8} \cdot \frac{\text{trace}(\Sigma_u)}{k}.$$

C.3. Generalized Forecast-Error Variance Decomposition (GFEVD)

The generalized FEVD of Pesaran and Shin (1998) used by Diebold and Yilmaz (2014) is computed as follows.

Define the moving-average representation:

$$X_{t+h} = \sum_{\ell=0}^h \Psi_\ell u_{t+h-\ell}.$$

¹⁹This rule ensures a minimum number of effective observations for stable VAR estimation.

²⁰This step prevents over-parameterized VARs and reduces numerical instability.

The H -step contribution of shocks from country j to forecast error variance of country i is:

$$\theta_{ij}(H) = \frac{\sum_{\ell=0}^{H-1} (e_i' \Psi_\ell \Sigma_u^\lambda e_j)^2}{\sum_{\ell=0}^{H-1} (e_i' \Psi_\ell \Sigma_u^\lambda \Psi_\ell' e_i)},$$

where e_i is a basis vector selecting country i . Rows are normalized:

$$\tilde{\theta}_{ij}(H) = \frac{\theta_{ij}(H)}{\sum_{j=1}^k \theta_{ij}(H)}.$$

Total spillover index. The Diebold–Yilmaz spillover measure is:

$$S^{\text{DY}}(H) = 100 \cdot \frac{\sum_{i \neq j} \tilde{\theta}_{ij}(H)}{k}.$$

C.4. Network Density Measure

As a complementary non-parametric interconnectedness metric, we compute the weighted network density based on instantaneous (within-window) rank correlations.

Correlation matrix. Let C denote the $k \times k$ Spearman correlation matrix of the standardized SHAP series in the window. Edges are retained if

$$|\rho_{ij}| \geq \tau, \quad \tau = 0.40.$$

Weighted density. Define:

$$D^{(w)} = \frac{\sum_{i < j} |\rho_{ij}| \cdot \mathbf{1}\{|\rho_{ij}| \geq \tau\}}{k(k-1)/2}.$$

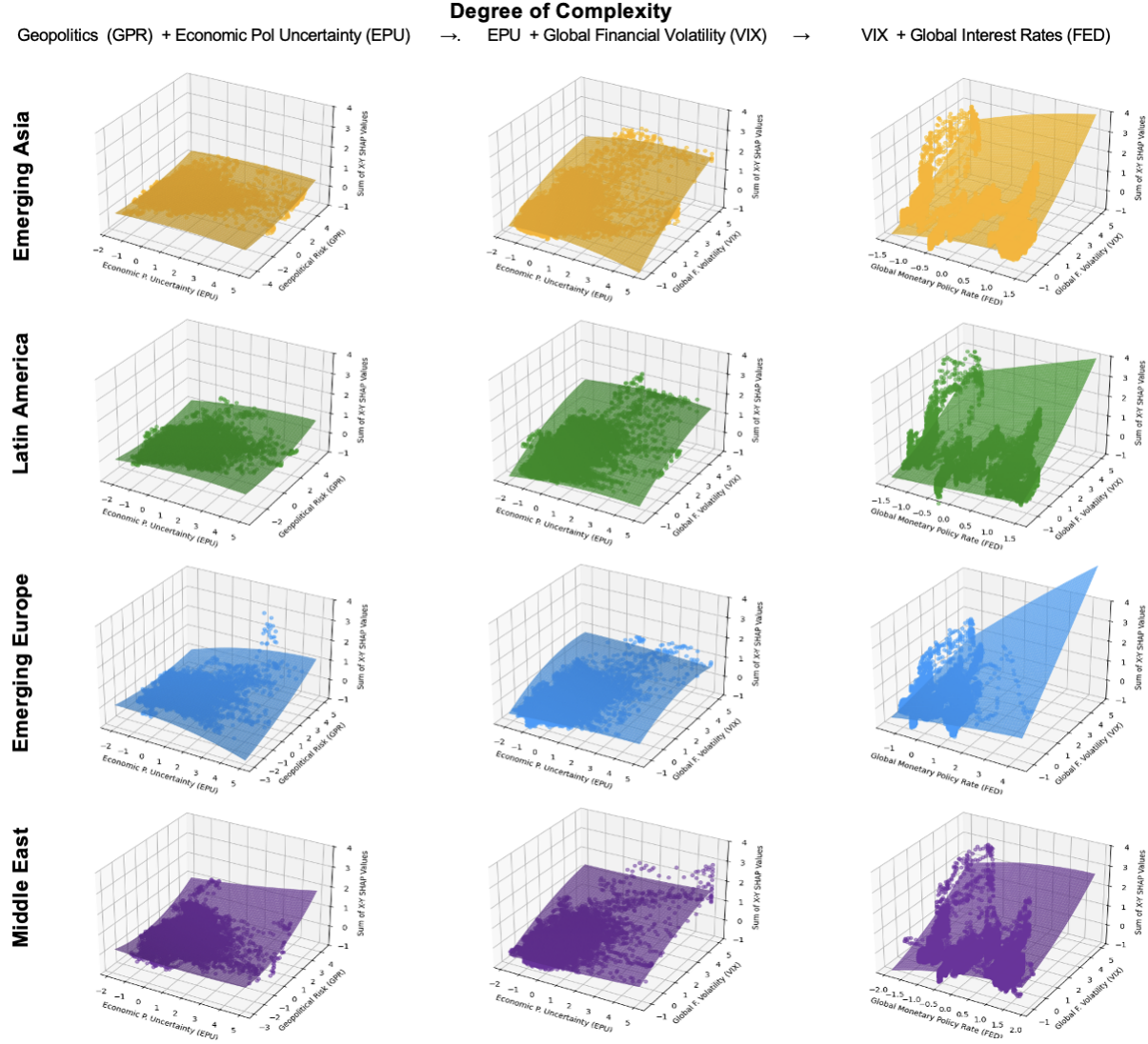
We scale:

$$\text{Density Index} = 100 \cdot D^{(w)}.$$

This index captures instantaneous synchronization without relying on lagged dynamics.

D APPENDIX D: Shap Dependence Plots

Figure 12: Shapley Contributions by Variable in Emerging Regions: Two-Factor SHAP Dependence Plots



Notes: The figure illustrates the combined impact of key predictors on sovereign CDS spreads across Emerging Market regions using two-factor SHAP dependence plots. The first column displays the joint influence of Geopolitical Risk (GPR) and Economic Policy Uncertainty (EPU). The middle onerow plots the joint contribution of EPU and Global Financial Volatility (VIX) The final one top row shows the joint effect of VIX and global monetary policy.